Snow Temperature Changes within a Seasonal Snowpack and Their Relationship to Turbulent Fluxes of Sensible and Latent Heat

SEAN P. BURNS,* NOAH P. MOLOTCH,+ MARK W. WILLIAMS,# JOHN F. KNOWLES,# BRIAN SEOK,@ RUSSELL K. MONSON,& ANDREW A. TURNIPSEED,** AND PETER D. BLANKEN++

** Department of Geography, University of Colorado Boulder, and National Center for Atmospheric Research, Boulder, Colorado*
+ Department of Geography, and Institute of Arctic and Alpine Research, University of Colorado Boulder, Boulder, Colorado, and Jet Propulsion Laboratory, California Institute of Technology, Pasadena, California
 # Department of Geography, and Institute of Arctic and Alpine Research, University of Colorado Boulder, Boulder, Colorado
@ Department of Atmospheric and Oceanic Sciences, and Institute of Arctic and Alpine Research, University of Colorado Boulder, Boulder, Colorado
& School of Natural Resources and the Environment, The University of Arizona, Tucson, Arizona
*** National Center for Atmospheric Research, Boulder, Colorado*
++ Department of Geography, University of Colorado Boulder, Boulder, Colorado

(Manuscript received 31 January 2013, in final form 9 August 2013)

ABSTRACT

Snowpack temperatures from a subalpine forest below Niwot Ridge, Colorado, are examined with respect to atmospheric conditions and the 30-min above-canopy and subcanopy eddy covariance fluxes of sensible Q_h and latent Q_e heat. In the lower snowpack, daily snow temperature changes greater than 1°C day^{-1} occurred about 1–2 times in late winter and early spring, which resulted in transitions to and from an isothermal snowpack. Though air temperature was a primary control on snowpack temperature, rapid snowpack warm-up events were sometimes preceded by strong downslope winds that kept the nighttime air (and canopy) temperature above freezing, thus increasing sensible heat and longwave radiative transfer from the canopy to the snowpack. There was an indication that water vapor condensation on the snow surface intensified the snowpack warm-up.

In late winter, subcanopy Q_h was typically between -10 and 10 W m^{-2} and rarely had a magnitude larger than 20 W m^{-2}. The direction of subcanopy Q_h was closely related to the canopy temperature and only weakly dependent on the time of day. The daytime subcanopy Q_h monthly frequency distribution was near normal, whereas the nighttime distribution was more peaked near zero with a large positive skewness. In contrast, above-canopy Q_h was larger in magnitude (100–400 W m^{-2}) and primarily warmed the forest–surface at night and cooled it during the day. Around midday, decoupling of subcanopy and above-canopy air led to an apparent cooling of the snow surface by sensible heat. Sources of uncertainty in the subcanopy eddy covariance flux measurements are suggested. Implications of the observed snowpack temperature changes for future climates are discussed.

1. Introduction

The accumulation of snow in the world's mountains provides a crucial source of water for both natural ecosystems and human society. Recent studies have shown that a warmer climate in the past five decades has affected both the amount of snow and timing of melt (Marty 2008; Mote et al. 2008) and that high-elevation areas in the midlatitudes are especially vulnerable to climatic warming (Pepin and Lundquist 2008; Clow 2010). Within a subalpine forest, the formation of a wet snowpack is an important event in the annual hydrologic and biological cycles because liquid water becomes available for trees, which initiates forest photosynthetic uptake of CO_2 (Monson et al. 2005; Hu et al. 2010). In an effort to better understand the meteorological conditions that affect snowmelt, energy budgets of snowpacks have been studied for nearly 80 yr. Many studies use slow-response meteorological instruments with empirical bulk aerodynamic formulas to estimate the turbulent energy fluxes (e.g., Niederdorfer 1933; Sverdrup 1936;

Corresponding author address: Sean P. Burns, NCAR/MMM, P.O. Box 3000, Boulder, CO 80307.
E-mail: sean@ucar.edu

DOI: 10.1175/JHM-D-13-026.1

Takahashi et al. 1956; Schlatter 1972; Male and Granger 1981; Marks and Dozier 1992; Marsh and Pomeroy 1996; Cline 1997; Hood et al. 1999; Hawkins and Walton 2007), whereas more recent studies use fast-response instrumentation with the eddy covariance technique to calculate turbulent energy exchange (Hicks and Martin 1972; McKay and Thurtell 1978; Yen 1995; Mahrt and Vickers 2005; Hayashi et al. 2005; Molotch et al. 2007; Marks et al. 2008; Reba et al. 2009; Mott et al. 2011). Marks et al. (2008) showed that, for a snowpack under a pine canopy, the mean differences calculated over several weeks between the eddy covariance and bulk-method fluxes were within 1–4 $W m^{-2}$ (with better agreement during the day than at night); hourly differences, however, were significantly larger than the long-term mean difference.

Most of the energy-budget studies listed above were in locations that are treeless or have sparse vegetation. Snowpacks within a forest are subject to a complicated radiative environment due to longwave radiant emission from tree boles and the overlying canopy, as well as shading the snowpack surface from incoming shortwave radiation (Male and Granger 1981; DeWalle and Rango 2008; Pomeroy et al. 2009; Lawler and Link 2011; Musselman et al. 2012a,b). Sicart et al. (2004) found that the effect of enhanced longwave and decreased shortwave radiation balanced the subcanopy daily net radiation for a wide range of canopy densities (in dense forests). In addition to radiative effects, forests shelter the snowpack from winds, thus reducing turbulent fluxes to and from the surface by an order of magnitude (Blanken et al. 1998). Canopies also intercept from 30% to 50% of the total snowfall, part of which sublimates back to the atmosphere before reaching the snowpack (Montesi et al. 2004; Molotch et al. 2007).

Within a snowpack, heat is transferred by a number of different processes, primarily, conduction through the interconnected snow crystals (Kaempfer et al. 2005), but also conduction through the interstitial air space, pressure pumping, and vapor transport driven by temperature gradients. The low thermal conductivity of the interstitial air makes snow an excellent insulator of the underlying soil (Sturm et al. 1997; Pomeroy and Brun 1999), which is an important consideration in land surface modeling (Strack et al. 2004; Ge and Gong 2010; Wang et al. 2010). Interstitial air mixing can also occur because of heat convection within a snowpack, which is driven by temperature differences due to spatial differences in snow depth or soil properties (Sturm and Johnson 1991).

The mixing of interstitial air by wind and pressure intrusions into the snowpack has typically been called ''pressure pumping'' (Colbeck 1989; Clarke and Waddington 1991; Massman et al. 1997; Bartlett and Lehning 2011). Recent results using CO_2 isotopes (within the same forest as the current study) have shown that short-lived, high-wind events enhance the diffusion process within the snowpack by up to 40%, with the upper snowpack being most affected (Bowling et al. 2009; Bowling and Massman 2011). For dry snow, CO_2 is useful for determining interstitial mixing because, unlike temperature, the interaction between CO_2 and the snow crystals is minimal. Our study will focus on temperature changes in the lower portion of the snowpack, where any external air that is mixed into the interstitial air space has come into thermal equilibrium with the surrounding snow.

Because of the close connection between snowpack temperature gradients and water vapor transport, which affects snow crystal structure, snow permeability, porosity, and tortuosity (Arons and Colbeck 1995; Kaempfer et al. 2005), monitoring snow temperature changes is critical to understanding the complicated relationship between snow crystal structure and gas transport within a snowpack. For example, the occurrence of melt–freeze cycles can introduce ice lenses into the snowpack (Colbeck 1991); the effect of ice layers on gas transport are not well understood and may enhance the horizontal transport of any trace gases released from the soil, while inhibiting vertical transport. Snow temperature changes, especially rapid changes, also affect the formation of both dry slab avalanches (McClung 1996; Schweizer et al. 2003) and wet snow avalanches (Armstrong 1976; Heywood 1989; McClung and Schaerer 2006) by directly modifying the snow grains and snowpack cohesiveness.

Turbulent fluxes comprise a large component of the snowpack energy balance in the premelt and ''ripening'' period and have been reported to control the internal energy content of subcanopy snow cover as melt accelerates in late spring (Marks et al. 2008). Though there is fairly strong consensus that turbulent fluxes above the snow surface are an important control on temperature changes within the snowpack, to the best of our knowledge, no previous study has attempted to link internal snowpack temperature changes to directly measured turbulent fluxes.

For the current study, eight seasons (2003–10) of snowpack temperature data from within a subalpine forest are examined with respect to atmospheric conditions (e.g., air temperature, humidity, and winds) and the turbulent surface fluxes of latent and sensible heat. We have focused on the temporal changes of these quantities, with an emphasis on explaining the environmental factors that most affect snowpack warm-ups prior to the initiation of spring snowmelt.

2. Snowpack heat transfer and energy budget

The relationships among snow crystal metamorphosis, snowpack water vapor, and snowpack temperature gradients are complex, and typically effective transport coefficients are used to account for the different processes (e.g., Langham 1981; Arons and Colbeck 1995; Domine et al. 2008). For example, the heat flux q_z at a point in the snowpack is assumed to be proportional to the vertical (z) snow temperature T_s gradient,

$$q_z = -k_{\mathrm{eff}}\frac{\partial T_s}{\partial z}, \tag{1}$$

where k_{eff} is the effective thermal conductivity, which varies between $0.03\,\mathrm{W\,m^{-1}\,K^{-1}}$ for fresh snow and $0.6\,\mathrm{W\,m^{-1}\,K^{-1}}$ for compacted snow (Sturm et al. 1997). Another important snow property is the effective thermal diffusivity ($\alpha_{\mathrm{eff}} = k_{\mathrm{eff}}/(\rho_s C_s)$, where ρ_s and C_s are the snow density ($\mathrm{kg\,m^{-3}}$) and ice heat capacity ($\mathrm{J\,kg^{-1}\,K^{-1}}$), respectively. Thermal diffusivity can also be determined from the second-order partial differential heat equation

$$\frac{\partial T_s}{\partial t} = \alpha_{\mathrm{eff}}\frac{\partial^2 T_s}{\partial z^2}. \tag{2}$$

Within the snow-science community, much effort has gone toward parameterizations of k_{eff} and α_{eff} with easily measured quantities such as snow density (e.g., Schlatter 1972; Pfeffer and Humphrey 1996; Brandt and Warren 1997; Sturm et al. 1997, 2002; Andreas et al. 2004; Oldroyd et al. 2013). Though our study does not specifically focus on internal snowpack heat transport processes, in the appendix we calculate α_{eff} from our snow temperature measurements to compare with recently published results by Oldroyd et al. (2013).

For a snowpack of depth h, where only vertical heat transport is considered and $z = 0$ corresponds to ground level, the snowpack energy budget (in $\mathrm{W\,m^{-2}}$) is

$$\frac{\partial}{\partial t}\left[\int_0^h \rho_s C_s (T_s - T_m)dz\right] + Q_m = R_{\mathrm{net}} + Q_{\mathrm{soil}} + Q_e + Q_h + Q_p. \tag{3}$$

The first term on the left side is the change with time of the so-called snowpack cold content (Q_{cc}, the energy required to bring a cold snowpack to the melting temperature T_m). The term Q_m represents internal energy changes due to melting and freezing of water within the snowpack. The terms on the right side are all related to surface exchanges of energy: net radiation R_{net}, ground heat flux Q_{soil}, latent heat flux Q_e, sensible heat flux Q_h, and energy added by precipitation Q_p. Following snow-research convention, a positive sign indicates energy added to the snowpack and a negative sign is energy extracted from the snowpack.

If the snowpack is within a forest, then the radiative and turbulent flux terms in Eq. (3) need to be evaluated in the subcanopy. Net radiation becomes particularly complicated. Our study does not have the necessary measurements to evaluate subcanopy radiation; however, we estimated subcanopy net longwave irradiance $(R^{\mathrm{s\text{-}c}}_{\mathrm{net}})_{\mathrm{LW}}$ with

$$(R^{\mathrm{s\text{-}c}}_{\mathrm{net}})_{\mathrm{LW}} = Q^{\downarrow}_{\mathrm{LW}}(1 - F_{\mathrm{srf\text{-}c}}) + \sigma(\varepsilon_f F_{\mathrm{srf\text{-}c}} T_c^4 - \varepsilon_{\mathrm{srf}} T_{\mathrm{srf}}^4), \tag{4}$$

where $Q^{\downarrow}_{\mathrm{LW}}$ is above-canopy incoming longwave radiation, $F_{\mathrm{srf\text{-}c}}$ is the view factor between the snowpack and forest, σ is the Stefan–Boltzmann constant, ε_f is canopy–tree emissivity, $\varepsilon_{\mathrm{srf}}$ is snow surface emissivity, T_c is canopy temperature, and T_{srf} is the snow surface temperature. More information about Eq. (4) and discussions about subcanopy net shortwave radiation are provided elsewhere (e.g., Sicart et al. 2004; DeWalle and Rango 2008; Pomeroy et al. 2009, and references therein).

3. Measurements

Measurements were primarily from the Niwot Ridge Subalpine Forest AmeriFlux site (NWT in Fig. 1) located in Colorado, approximately 8 km east of the Continental Divide at 3050-m elevation (Table 1). Typical tree heights at NWT are between 11 and 13 m, tree density is around $0.4\,\mathrm{trees\,m^{-2}}$, leaf area index is 3.8–$4.2\,\mathrm{m^2\,m^{-2}}$, and canopy gap fraction is 18% (Turnipseed et al. 2002). Turnipseed et al. (2002) supplies additional information about long-term measurements of radiation, soil heat flux, soil temperature, and soil moisture content. A summary of recent changes to the soil temperature and moisture measurements at NWT are described below. The NWT AmeriFlux data were downloaded on 28 February 2013 from http://urquell.colorado.edu/data_ameriflux/. To expand the scale of the NWT observations, we also used data from the Soddie site on Niwot Ridge at 3345 m elevation (Williams et al. 2009), as well as meteorological data from the National Oceanic and Atmospheric Administration (NOAA) Table Mountain Surface Radiation Budget Network (SURFRAD) site (NOAA 2012) at 1689-m elevation and about 30 km east of NWT in the lower foothills–plains boundary. Table 1 contains additional details of all the measurement locations and variables. Unless

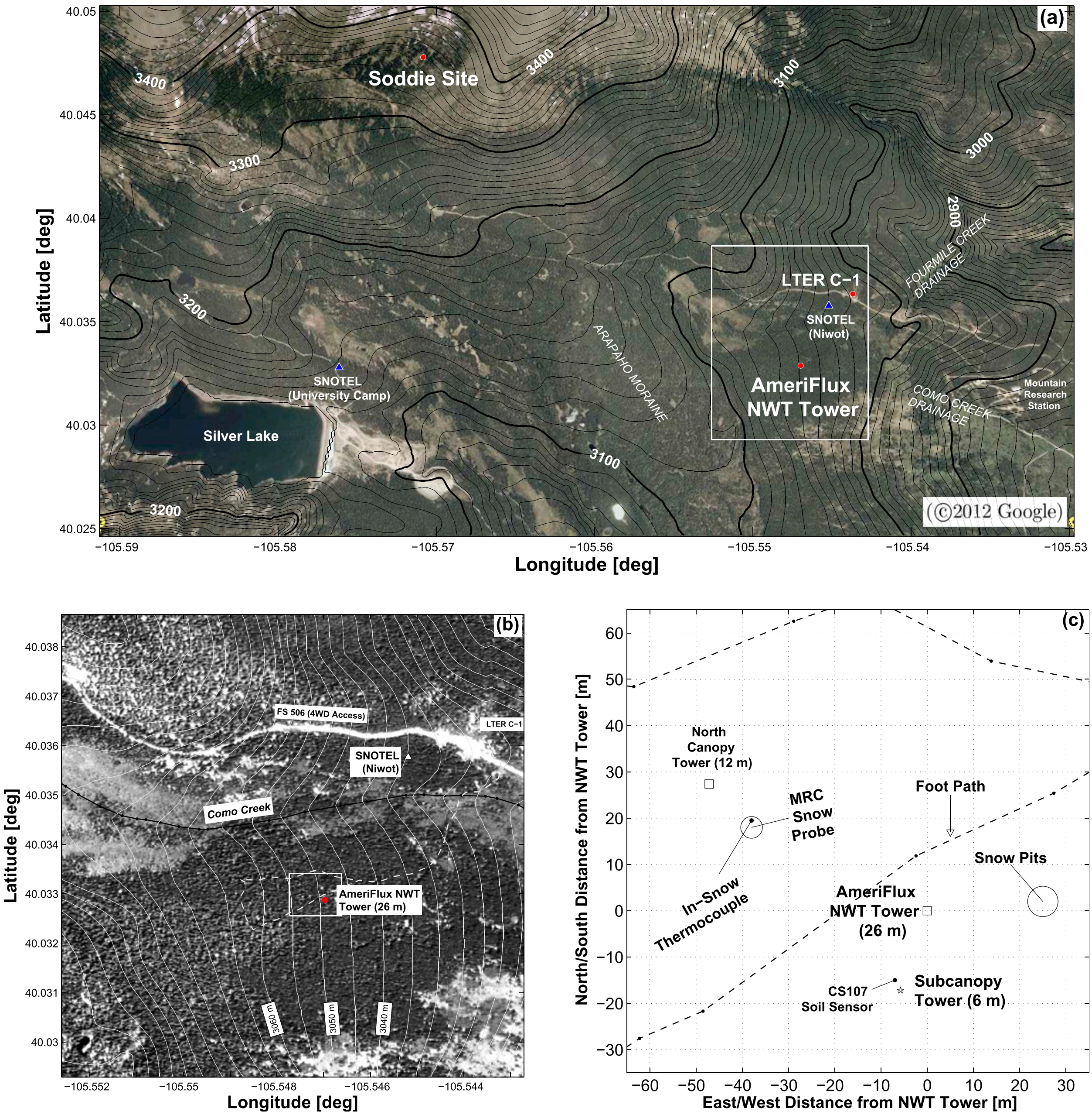

FIG. 1. Maps showing the instruments and topography near NWT. (a) The red circles show the Soddie site, the NWT tower, and the LTER C-1 site, while the triangles show SNOTEL sites 663 (Niwot) and 838 (University Camp). The background image is from Google Maps (©2012 Google) and the elevation contours at 10-m intervals are from the U.S. Geologic Survey 7.5-min digital elevation model. (b) The white box in (a) is expanded and includes elevation contours at 5-m intervals. (c) Map showing a 100-m^2 area around the NWT tower with the location of the MRC snow probe (between years 2006–2010) as well as other sensor locations.

otherwise noted, 30-min periods were used for turbulent flux calculations and other statistics.

a. Turbulent and radiative fluxes

Turbulent fluxes of sensible and latent heat were measured at the NWT site by the eddy covariance technique with three-dimensional sonic anemometers (Campbell Scientific, model CSAT3) measuring the vertical wind and temperature fluctuations. For above-canopy sensible heat flux (at 21.5 m), corrections to the sonic temperature following Burns et al. (2012) were applied. For latent heat flux, a krypton hygrometer (Campbell Scientific, model KH2O) was the primary instrument used to measure the humidity fluctuations.

However, a closed-path infrared gas analyzer (IRGA; LI-COR, model LI-6262) with an inlet at 21.5 m was used when the krypton hygrometer was not available (Monson et al. 2002; Turnipseed et al. 2002; Molotch et al. 2009). In the subcanopy, water vapor fluctuations were measured at 2.5 m with an open-path IRGA (LI-COR, model LI-7500) and collocated CSAT3 on the accompanying 6-m subcanopy flux tower (Molotch et al. 2007). The eddy covariance fluxes were calculated using standard methods (e.g., Aubinet et al. 2000; Massman and Lee 2002; Foken et al. 2012), but without corrections for high-frequency signal attenuation or for open-path IRGA sensor heating (Burba et al. 2008). The open-path Burba correction for latent heat flux is a factor of 100 smaller than for CO_2 flux and is only significant if the latent heat flux is accumulated over a long period (Reverter et al. 2010). Latent heat flux was calculated using latent heat of vaporization as a function of temperature (Bolton 1980); however, we did not use the latent heat of sublimation, which results in a slight ($\approx$10%) underestimation of the true flux during cold periods when sublimation was occurring.

Above-canopy net radiation (R_{net}) was measured on the NWT tower at 25 m with a net radiometer [Radiation and Energy Balance Systems (REBS), model Q*7.1]. The above-canopy surface energy budget closure approaches 80%–90% as long as there is sufficient turbulent mixing and an empirical correction is applied to the CSAT3 sensible heat flux measurements in high-wind conditions (Burns et al. 2012).

b. Snowpack and soil temperature and soil moisture

Snowpack and soil temperatures were measured in various locations at the site by thermocouples, thermistors, and a 2-m polycarbonate rod with thermistors embedded every 10 cm [Measurement Research Corporation (MRC) model TP101 probe, hereafter MRC probe]. The polycarbonate material has a thermal conductivity similar to wood ($0.3\ \mathrm{W\,m^{-1}\,K^{-1}}$). The MRC probe was inserted approximately 20–30 cm into the soil, and the snow was allowed to naturally accumulate around the probe. Starting in the fall of 2005, the MRC probe was located about 60 cm from the nearest tree bole at the western edge of a small forest opening (15 m $\times$ 10 m) between the North Canopy tower and the NWT tower (Fig. 1c). The probe was supported from above by fishing line attached to nearby trees and marked so snow depth at the probe could be recorded. Prior to the fall of 2005, the MRC probe was at other locations near the NWT tower. A one point, in situ calibration was conducted using the period when the snowpack was isothermal (at 0°C) to determine a constant offset that was universally applied to all thermistors within the MRC probe. During the isothermal period, the standard deviation of 30-min MRC temperature from zero for the in-snow sensors was 0.03°C.

In October 2005, a soil moisture sensor (Campbell Scientific, model CS616) and soil temperature sensor (Campbell Scientific, model CS107) were installed horizontally at a depth of 5 cm near the 6-m subcanopy tower. Prior to deployment, the CS107 thermistor was calibrated against a NIST-standard temperature sensor at the National Center for Atmospheric Research (NCAR) Integrated Surface Flux System (ISFS) calibration facility.

In October 2008, several type-T copper–constantan thermocouples (Campbell Scientific, model A3537) were added within a few meters of the MRC snow probes in a vertical profile at 20 cm below ground level, ground level, and 20 cm above ground level. The thermocouple lead wires were laid along the ground to not disturb the upper snow surface, and data were collected with a multiplexer specifically designed to measure thermocouple temperatures (Campbell Scientific, model AM25T). These thermocouples were used for validation of the MRC probe accuracy (section 4a).

Snow temperature was also measured at the Soddie site on Niwot Ridge, located 2.5 km northwest and 300 m higher in elevation than the NWT AmeriFlux site (Fig. 1a). The Soddie snow temperature was measured at multiple heights between the ground and 250 cm with type-E chromel–constantan thermocouples from a 2.5 m mast located in an open meadow just below tree line (Seok et al. 2009). The specific measurement heights varied from year to year. The Soddie site has a south-facing aspect, whereas the NWT site is primarily eastward facing.

c. Snowpack properties and other ancillary data

Snow depth was continuously measured by an ultrasonic distance sensor (Campbell Scientific, model SR50-L) at the C-1 site (around 500 m northeast of the NWT AmeriFlux tower) by the Niwot Ridge Long Term Ecological Research (LTER) Mountain Climate Program. Every few weeks, snow depth was also recorded by visually reading the marked depths on the MRC snow probes during site visits. Continuous snow depth (and mean snowpack density) was recorded at the Natural Resources Conservation Service (NRCS) Snowpack Telemetry (SNOTEL) site closest to the NWT tower (Niwot, site 663, 350 m northeast of NWT). Snow depth at the Soddie site was derived using snow depth from SNOTEL site 838 (University Camp), as described in Seok et al. (2009). Snow density at the NWT site typically varies from around $200\ \mathrm{kg\,m^{-3}}$ in late January to over $350\ \mathrm{kg\,m^{-3}}$ during the melt period (Bowling and

TABLE 1. A summary of instrumentation and variables from the NWT AmeriFlux, LTER C-1, Soddie, SNOTEL, and NOAA SURFRAD sites used in our study.

Location or variable[a]	Symbol	Sensor type	Manufacturer make/model	Sensor height(s) (cm)	Data period[b]	Additional comments
NWT AmeriFlux site (location: 40.033°N, 105.547°W; elevation: 3050 m)						
Air temperature and relative humidity (RH) (°C, %)	T_a, RH	Platinum resistance thermometer, capacitive humidity sensor	Vaisala, HMP35D/45D	200, 800, 2150	Feb 2005 to Apr 2010	Slow-response sensor within a mechanically aspirated housing.
Barometric pressure (kPa)	P	Silicon capacitive sensor	Vaisala, PTB-101B	1200	Feb 2005 to Apr 2010	Used along with T_a and RH to calculate specific humidity q and dewpoint temperature T_d.
Net radiation (W m^{-2})	R_{net}	Thermopile	REBS, Q*7.1	2550	Feb 2005 to Apr 2010	
Snow and soil temperature (°C)	T_s, T_{soil}	Thermistor	MRC probe	−10 to 190 (10-cm spacing)	Feb 2003 to Apr 2010	After Oct 2005, deployed at one location near NWT tower (see Fig. 1).
		Thermistor	Campbell Scientific, CS107	−5	Feb 2006 to Apr 2010	Installed horizontally.
		Thermocouple (type T)	Campbell Scientific, A3537	−20, 0, 20	Feb 2008 to Apr 2010	
Soil heat flux (W m^{-2})	Q_{soil}	Thermopile	REBS, HFT-1	−10	Feb 2005 to Apr 2010	The average from multiple sensors was used.
Soil volumetric water content [$V_{H_2O}(V_{soil})^{-1}$, m^3 m^{-3}]	VWC	Electromagnetic conductivity	Campbell Scientific, CS616	−5	Feb–Mar 2006	Installed horizontally, units are volume of water (V_{H_2O}) per volume soil (V_{soil}).
Wind speed and direction (m s^{-1}, deg. from true north)	WS, WD	Sonic anemometer	Campbell Scientific, CSAT3	256, 570, 2150	Feb 2005 to Apr 2010	
3D wind and temperature fluctuations[c] (m s^{-1}, °C)	u', v', w', T'_{sonic}	Sonic anemometer	Campbell Scientific, CSAT3	256, 2150	Feb 2005 to Apr 2010	CSAT3 vertical wind fluctuations (w') were used to calculate turbulent fluxes.
Sensible heat flux (W m^{-2})	Q_h	Sonic anemometer + thermocouple (type E)	Campbell Scientific, CSAT3 + Omega	2150, 256	Feb 2005 to Apr 2010	In high winds, a thermocouple was used to calculate 2150 cm Q_h following Burns et al. (2012).
Latent heat flux (W m^{-2})	Q_e	Sonic anemometer + Krypton hygrometer (2150 cm), open-path IRGA (256 cm)	Campbell Scientific, KH2O, LI-COR, LI-7500	2150, 256	Feb 2005 to Apr 2010	A closed-path IRGA (LI-COR, LI-6262) was used at 2150 cm whenever the KH2O sensor was not available.
LTER C-1 (location: 40.037°N, 105.544°W; elevation: 3021 m)						
Snow depth (cm)	h	Ultrasonic sensor	Campbell Scientific, SR50-L	≈300	Feb 2003 to Apr 2010	
Soil volumetric water content [$V_{H_2O}(V_{soil})^{-1}$, m^3 m^{-3}]	VWC	Electromagnetic conductivity	Campbell Scientific, CS615	−15 to 0	Feb–Mar 2006	Installed vertically.

TABLE 1. (*Continued*)

Location or variable[a]	Symbol	Sensor type	Manufacturer make/model	Sensor height(s) (cm)	Data period[b]	Additional comments
Soddie (location: 40.048°N, 105.571°W; elevation: 3345 m)						
Snow depth (cm)	h	Calculated			Feb 2006 to Apr 2009	See Seok et al. (2009) for details.
Snow temperature (°C)	T_s	Thermocouple (type E)	Omega Engineering	10–150	Feb 2006 to Apr 2009	Sensor heights varied from year to year, year 2008 was not used.
SNOTEL, site 663, Niwot (location: 40.036°N, 105.545°W; elevation: 3030 m)						
Snow depth (cm)	h	Ultrasonic sensor	Judd Communications, depth sensor	480	Feb 2006 to Apr 2010	See http://www.wcc.nrcs.usda.gov/.
Snow density (kg m^{-3})	ρ_s	Pressure-sensing snow pillow	General Electric, Druck PMP 317		Feb–Mar 2006	See http://www.wcc.nrcs.usda.gov/.
SURFRAD at Table Mountain (location: 40.13°N, 105.24°W; elevation: 1689 m)						
Air temperature and relative humidity (°C, %)	T_a, RH	Platinum resistance, capacitive humidity	Vaisala	100	Feb–Mar 2006	See http://www.esrl.noaa.gov/gmd/grad/surfrad/.

[a] Variable units are shown below the variables in parentheses.
[b] This is the time period used for these data within the study.
[c] The values u', v', w', are wind fluctuations in the streamwise, crosswind, and vertical directions; $T'_{\rm sonic}$ represents sonic temperature fluctuations.

Massman 2011). For this study, the continuous snowpack density from the Niwot SNOTEL site was used.

Air temperature T_a and humidity measurements were made at the 2-, 8-, and 21.5-m levels on the NWT tower by slow-response temperature–humidity sensors (Vaisala, models HMP35D and HMP45D) housed within mechanically aspirated radiation shields. At the SURFRAD site, air temperature and humidity were measured by a Vaisala temperature–humidity sensor within a naturally ventilated radiation shield at 10 m above the ground.

4. Results

a. *Validation of MRC probe temperature measurements*

The snow and soil temperature sensors in our study measured similar temperature changes and trends (Fig. 2). Because the upper portion of the MRC probe protruded above the snow surface, we were concerned with along-probe temperature conduction affecting the MRC snow temperature measurements. Though probes similar to the MRC probe have been used in other snow studies (e.g., Fierz 2011; Oldroyd et al. 2013), we chose to check the validity of the MRC probe data using other nearby temperature measurements (Fig. 1). Despite being in different locations, $T_{\rm soil}$ from the CS107 sensor compared to the −5-cm level of the MRC snow probe have a mean difference and standard deviation of 0.04 ±0.09°C and a slope of 0.97 (Fig. 3a). As another quality check, the independent thermocouple installed at 20-cm height in fall 2008 agrees well with T_s from the MRC probe (Fig. 3b). The year-to-year T_s differences between the thermocouple and MRC probe could be due to the thermocouple height changing slightly within the snowpack, as well as spatial differences in snow temperature. The other supplemental thermocouples near the MRC snow probe produced similar comparison results.

b. *Snow and soil temperature*

In midwinter, snow temperature from the MRC probe at a height of 35 cm typically reached a minimum of around −5°C, whereas the soil temperature rarely went below −1°C (Fig. 2). Snow temperature changes with time ($\Delta T_s/\Delta t$) were calculated over each 24-h period, and the magnitude of $\Delta T_s/\Delta t$ at 35-cm height was typically smaller than 0.5°C day^{-1}. In most years, there were brief periods between mid-February and early April when T_s changed at a rate greater than 1°C day^{-1} and the snowpack rapidly warmed, sometimes becoming isothermal at 0°C. These snowpack warm-up events (identified by the vertical dashed lines in Fig. 2 and listed in Table 2) could

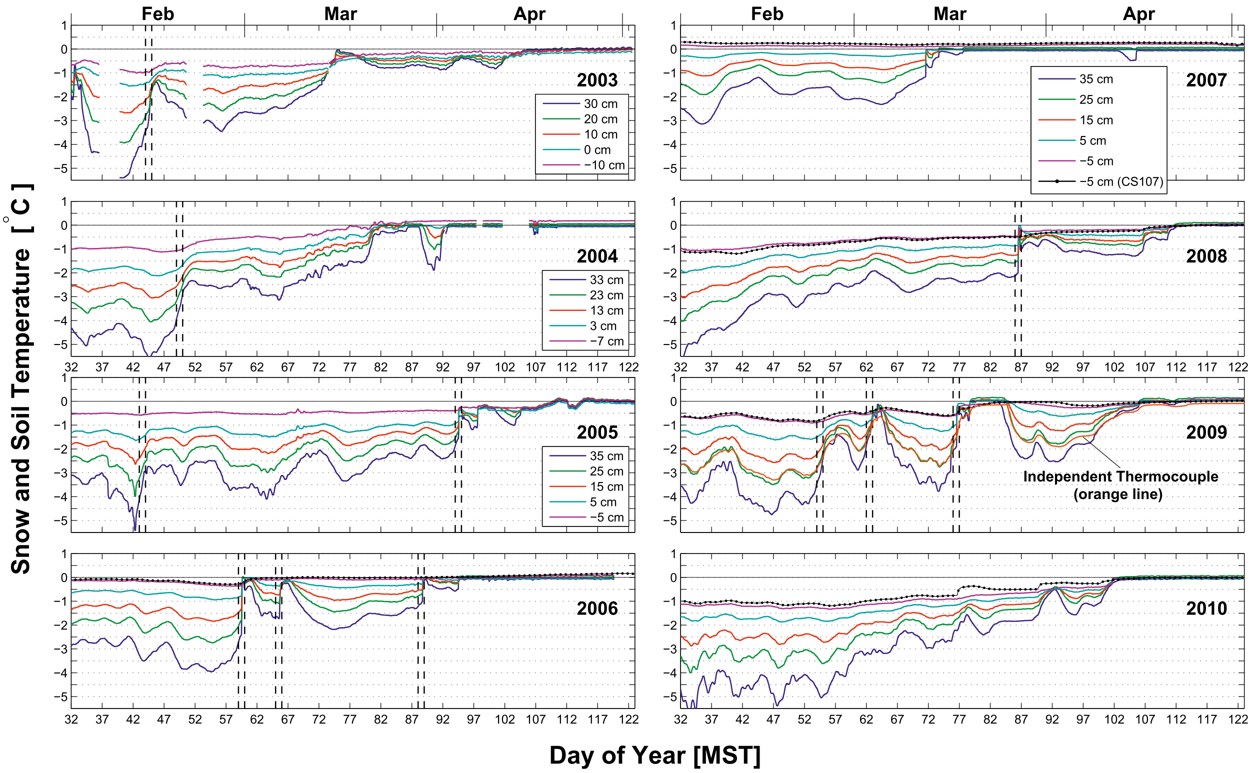

FIG. 2. Time series of 30-min average snow and soil temperatures for years 2003–10. For 2006–10, the MRC snow temperature probe was not moved and the 2007 legend applies to these years. For 2006–10, an independent soil temperature sensor (CS107 thermistor, see text for details) is shown as a black line. For 2009, an independent snowpack thermocouple located at 20 cm above the ground and near the snow temperature probe is shown as an orange line. Dashed vertical lines indicate snowpack warming events.

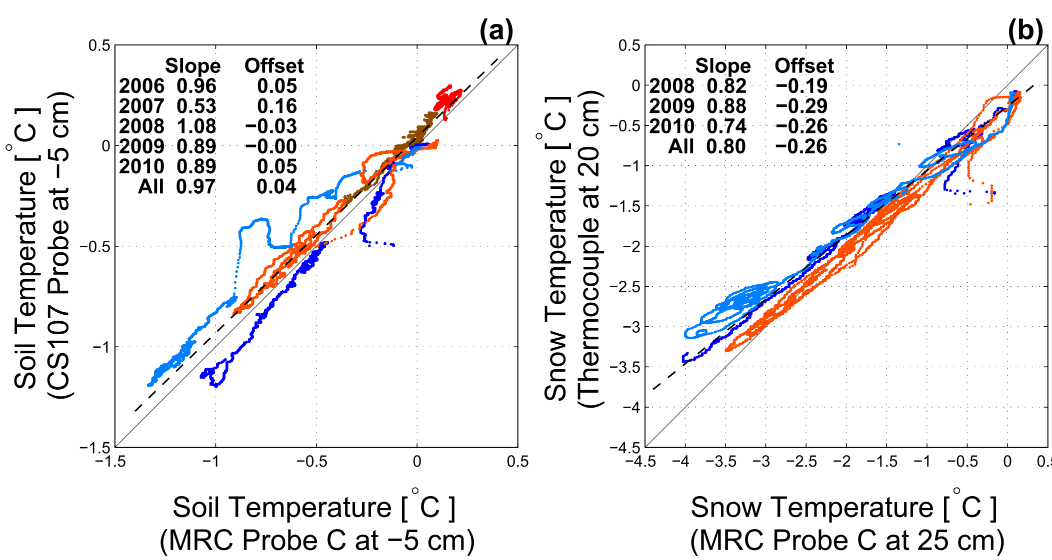

FIG. 3. Temperature measured with the MRC snow probe compared to (a) an independent soil temperature sensor (CS107 thermistor) and (b) a thermocouple within the snowpack. These are 30-min mean values between days of year 32 and 123, where each color represents a different year as specified in the legend. The slope and offset for each year is shown in the upper-left corner, and the dashed line is a linear fit through the data from all available years. The CS107 soil temperature sensor is located about 50 m southeast of the MRC probe (see Fig. 1c for sensor locations).

TABLE 2. Statistics from the dates when the 24-h finite difference of snow temperature ($\Delta T_s/\Delta t$) is greater than 1°C day^{-1}. The sensible Q_h and latent Q_e heat fluxes and net radiation R_{net} use the snow-research sign convention, which is positive for energy transport toward the surface (i.e., warming of the snowpack). NA indicates missing data.

Year		2003	2004	2005	2005	2006	2006	2006	2008	2009	2009	2009
Date		2/13	2/18	2/12	4/04	2/28	3/06	3/29	3/26	2/23	3/03	3/17
Day of year		44	49	43	94	59	65	88	86	54	62	76
Time (MST)[a]		1400–1600	Gradual	Gradual	1200–1300	1200–1400	1400–1800	1600–1800	1200–1400	Gradual	Gradual	1300–1500
$\Delta T_s/\Delta t$[b] (°C day^{-1})		1.70	1.07	1.16	1.25	2.30	1.29	1.08	1.09	1.08	1.28	1.53
Snow depth[c] [h, (cm)]		NA	NA	NA	NA	81.4	76.4	108.4	96.9	72.5	70.5	70.0
Snow density[d] [ρ_s, (kg m^{-3})]		NA	NA	NA	NA	273.7	299.2	299.6	300.8	264.8	283.3	299.2
25-m R_{net} (W m^{-2})	Day[e]	250.7	515.5	236.5	400.5	545.7	592.0	510.5	678.7	393.4	586.1	586.1
	Night[f]	−39.7	−84.2	−19.6	−84.9	−72.7	−89.0	−65.5	−66.4	−53.7	−83.1	−64.8
2-m T_a (°C)	Day[e]	3.8	7.9	2.7	6.5	7.1	8.0	7.0	6.5	3.3	6.4	6.6
	Night[f]	−4.4	0.14	−2.4	0.94	0.50	−1.9	−3.7	0.12	−1.8	2.3	1.2
21.5-m WS (m s^{-1})	Day[e]	2.2	8.2	3.9	3.4	12.5	4.0	4.2	6.8	11.8	8.6	5.1
	Night[f]	2.2	8.9	1.7	3.8	8.2	3.1	1.9	7.2	3.7	12.9	7.0
21.5-m Q_h (W m^{-2})	Day[e]	−132.3	−326.2	−159.1	−280.5	−442.9	−347.0	−328.4	−484.2	−259.7	−388.6	−406.0
	Night[f]	22.4	79.5	11.7	91.1	77.4	119.0	47.4	69.2	48.2	79.4	70.6
21.5-m Q_e (W m^{-2})	Day[e]	−21.8	−30.1	−16.0	−21.7	−49.7	−42.1	−16.4	−55.3	−41.3	−43.1	−32.1
	Night[f]	0.53	−3.2	−2.5	−8.8	−35.2	−16.2	1.5	−13.4	6.8	−31.2	−13.3
2.56-m Q_h (W m^{-2})	Day[e]	6.2	NA	1.1	5.8	33.0	12.5	5.1	−3.3	3.1	6.2	3.5
	Night[f]	0.44	NA	0.43	5.5	18.4	6.5	0.83	8.4	4.1	18.5	14.8
2.56-m Q_e (W m^{-2})	Day[e]	−0.38	NA	−7.8	−9.5	−13.3	−11.6	−6.4	−21.2	−6.4	−15.4	−16.0
	Night[f]	NA	NA	−0.15	−0.44	−13.0	−5.0	−0.16	−4.9	−4.1	−12.6	−12.7

[a] The time range listed is MST period when the 35-cm snow temperature T_s is warming most rapidly. If there was no sharp change in T_s, then the designation gradual is used.
[b] The 24-h finite difference of snow temperature ($\Delta T_s/\Delta t$) is calculated using the 35-cm level between midnight and midnight.
[c] Snow depth h is estimated at the MRC probe from the continuous C-1 snow depth sensor.
[d] Snow density ρ_s from SNOTEL site 663 (Niwot).
[e] The day period is from 1100 to 1400 MST on the day of the snowpack warm-up.
[f] The night period is from 2400 to 400 MST on the morning prior to the snowpack warm-up.

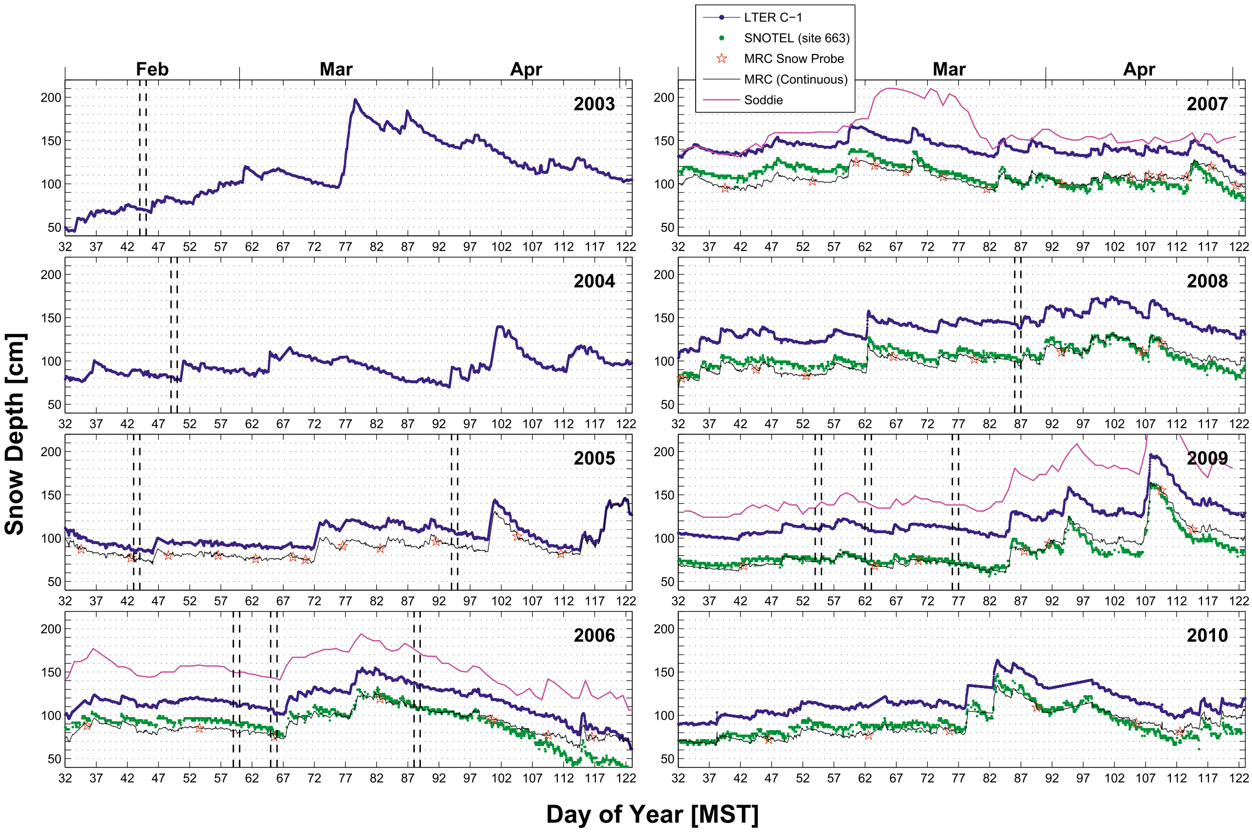

FIG. 4. Snow depth measured at LTER C-1, SNOTEL and at the MRC snow probe as specified in the legend. The snow depth measurements at the MRC snow probe were recorded during site visits (based on markings on the snow probe) and are combined with continuous C-1 snow depth to create a continuous snow depth at the MRC snow probe (thin black line). For years 2006, 2007 and 2009, snow depth at the Soddie site is shown. Dashed vertical lines indicate significant snowpack warming events as shown in Fig. 2.

occur several times before the start of spring snowmelt. After warming, the snowpack typically reverted back to having vertical T_s gradients; however, the magnitude of the T_s gradients following such an event was often smaller than the pre-event T_s gradients (e.g., warm-up events in years 2003, 2004, 2006, 2008, and 2009).

To better understand $\Delta T_s/\Delta t$, it was necessary to know the snow depth at the MRC probe. To create a continuous snow depth time series at the MRC probe, the hourly snow depth measurements from C-1 were linearly adjusted to the periodic snow depth measurements at the MRC probe (Fig. 4). The 35-cm-level $\Delta T_s/\Delta t$ variation with snow depth was either positive (snowpack warming) or negative (snowpack cooling) for any snow depth (Fig. 5a). However, for deeper snowpacks, the magnitude of $\Delta T_s/\Delta t$ was reduced because of the insulating properties of snow, which creates the pyramid-like pattern in Fig. 5a. We quantified the amount of snowpack heating and cooling by calculating the standard deviation (STDV) of $\Delta T_s/\Delta t$ (0.30°C day^{-1} for the 35-cm level as shown in Fig. 5a). For our study, the periods of interest are the points marked by open circles in Fig. 5a, where the snowpack was deep, but rapid snowpack warm-ups occurred.

Up to this point the focus has been on the 35-cm level, however, other heights within the snowpack also need to be considered. To achieve this, we composited 5 yr of February–April data for each of the MRC probe levels, and examined how the mean and STDV of $\Delta T_s/\Delta t$ changed for each level (Fig. 5b). As one would expect, the air above the snowpack (i.e., $z > 150$ cm) warmed between 1 February and 30 April, and we found an average warming rate of about 0.09°C day^{-1} (Fig. 5b). Closer to the ground, the mean of $\Delta T_s/\Delta t$ trended toward zero because the snow insulates the lower snowpack and soil (i.e., from early February to the end of April, the soil temperature does not change very much).

If the diurnal air temperature changes near the top of the snowpack influenced T_s, then the magnitude of the STDV of $\Delta T_s/\Delta t$ should increase (Reusser and Zehe 2011). Similar to the mean value of $\Delta T_s/\Delta t$, the STDV of $\Delta T_s/\Delta t$ was much smaller within the snowpack than in the air (Fig. 5b). The levels least affected by the diurnal air temperature changes were those below

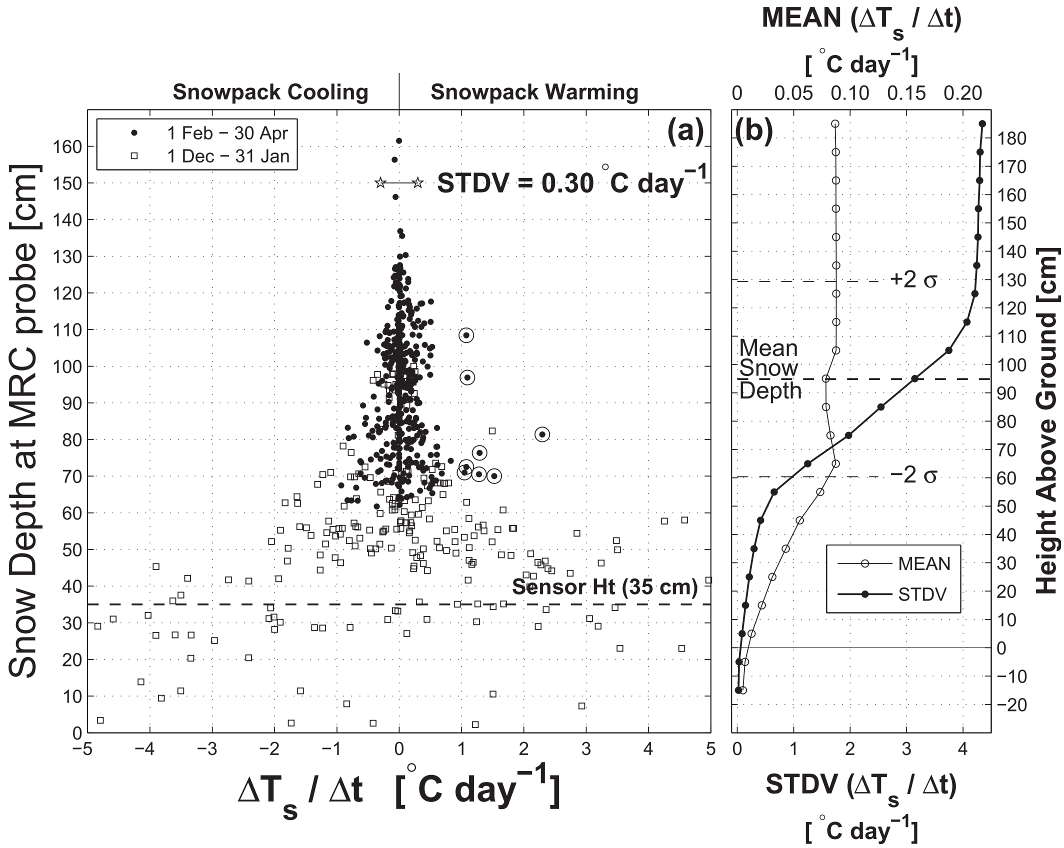

FIG. 5. (a) The 24-h finite difference of snow temperature ($\Delta T_s/\Delta t$) for years 2006–10 at 35 cm above the ground vs snow depth where $\pm$STDV of $\Delta T_s/\Delta t$ is shown by the horizontal line at a snow depth of 150 cm; in addition, periods when the snowpack is still forming (i.e., December and January) are included, as described by the legend. Time periods between 1 February and 30 April with $\Delta T_s/\Delta t > 1°\text{C day}^{-1}$ are highlighted by open circles. (b) The vertical profile of the mean (upper axis) and STDV (lower axis) of $\Delta T_s/\Delta t$ for years 2006–2010 for the MRC probe between 1 February and 30 April. The horizontal lines show the ground–snow interface at $z = 0$ (solid line), mean snow depth at $z \approx 95$ cm (dashed line), and ± 2 STDVs (2σ) around the mean snow depth (dashed lines).

about 60 cm (or about 30 cm below the mean snow depth). Not surprisingly, this region is directly related to the range of snow depths that we estimated by twice the standard deviation ($\pm 2\sigma$) of snow depth. Because we are interested in the region of the snowpack that was least influenced by diurnal air temperature changes (and pressure pumping effects), we focus on the lower snowpack (i.e., $z < \approx 60$ cm) for the remainder of our study.

c. *Snow temperature comparison with Soddie*

The comparison between the MRC snow probe temperature with those near the tree line at the Soddie site show remarkable agreement in the timing and magnitude of the snow temperature changes (Fig. 6). The late winter snowpack at the Soddie site was typically 60–70 cm deeper than at the NWT site (Figs. 4, 6). Despite slightly colder air temperatures at Soddie, T_s near the bottom of the deeper Soddie snowpack was typically about 1°–2°C warmer than at NWT. For 2007, T_s in the lower snowpack at Soddie was slightly colder than other years, presumably because of the extremely cold air mass that influenced T_s in early February (Fig. 6b). The insulating properties of snow that keep the soil near 0°C in winter will also sustain lower temperatures within the snowpack after they become established.

d. *Wintertime above- and subcanopy energy fluxes*

The mean monthly diel cycles of above-canopy sensible and latent heat fluxes (Fig. 7a) were an order of magnitude larger than the corresponding subcanopy fluxes (Fig. 8a). The subcanopy turbulent fluxes were also smaller than these same fluxes measured above the tree line on Niwot Ridge at 3480-m elevation at 3-m height (e.g., Blanken et al. 2009; Knowles et al. 2012).

From the above-canopy measurements, we found that net radiation warmed the surface during the daytime (including the snow and tree boles, branches, and needles) and cooled it by longwave radiation at

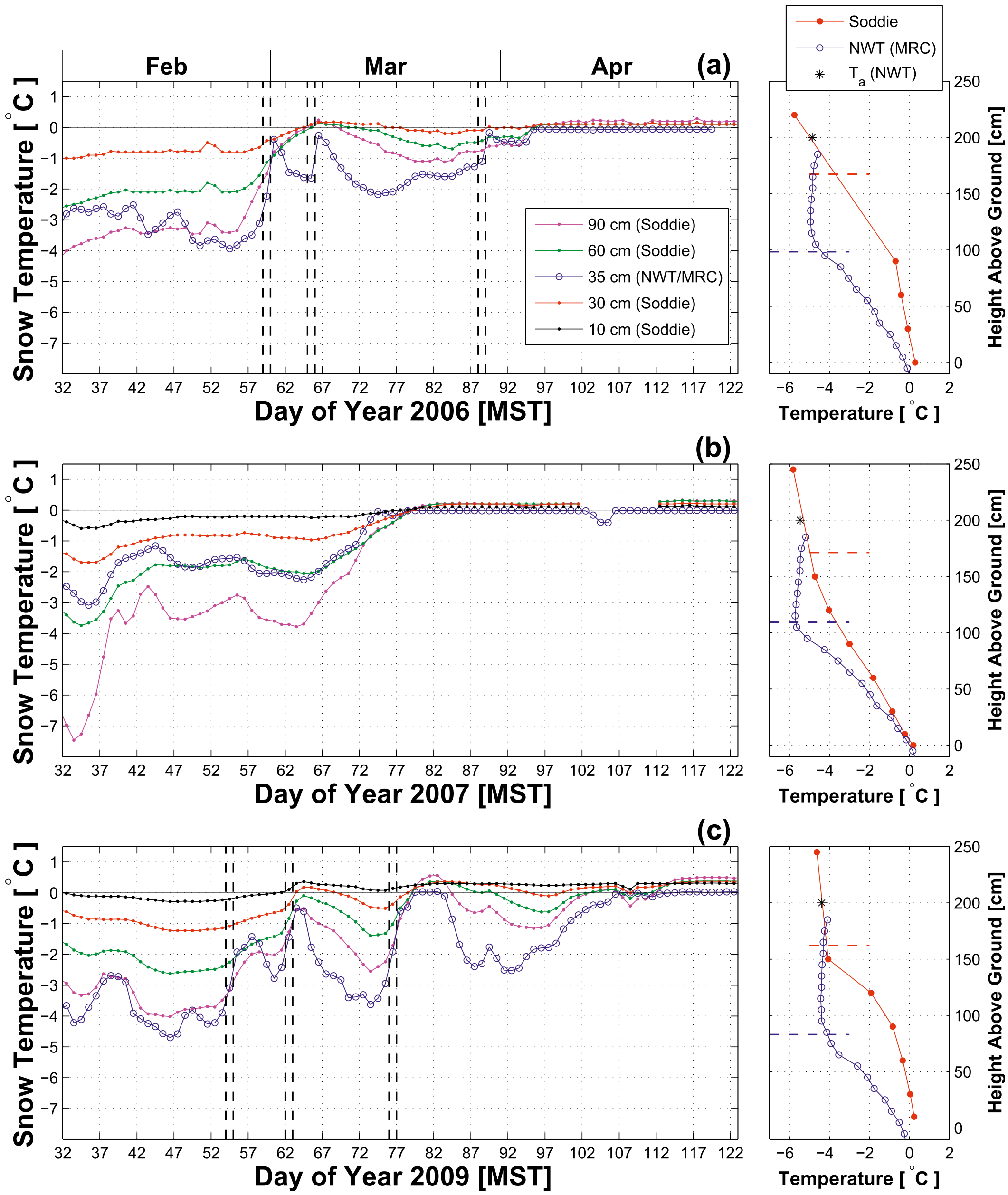

FIG. 6. (left) Time series of snow temperature measured at the Soddie site and the AmeriFlux NWT site (the MRC snow probe at 35 cm) for (a) 2006, (b) 2007, and (c) 2009. Sensor heights above the ground are in the legend and change slightly from year to year. These are 24-h mean values calculated from midnight-to-midnight. The 35-cm MRC snow temperature is the same as that in Fig. 2. (right) The mean temperature profiles at each site for the 4 weeks prior to the snowpack becoming isothermal for the years in (a)–(c). Dashed horizontal lines indicate the mean snow depth over that period at NWT (blue) and Soddie (red). The 2-m air temperature T_a was measured on the NWT tower.

night (Fig. 7a). The radiative flux was primarily balanced by the sensible heat flux. As the season progressed from February to April, midday R_{net} changed from around 400 to nearly 600 W m^{-2}, while there were correspondingly smaller increases in the magnitude of Q_h and Q_e (presumably because a portion of the net radiative energy was being used to melt the snow). The latent heat flux was a small (but consistent) cooling influence on the snowpack surface because of sublimation and evaporation. Frequency distributions of daytime Q_h are broad and indicate surface cooling (Fig. 7b), while the nocturnal Q_h frequency distributions have a smaller

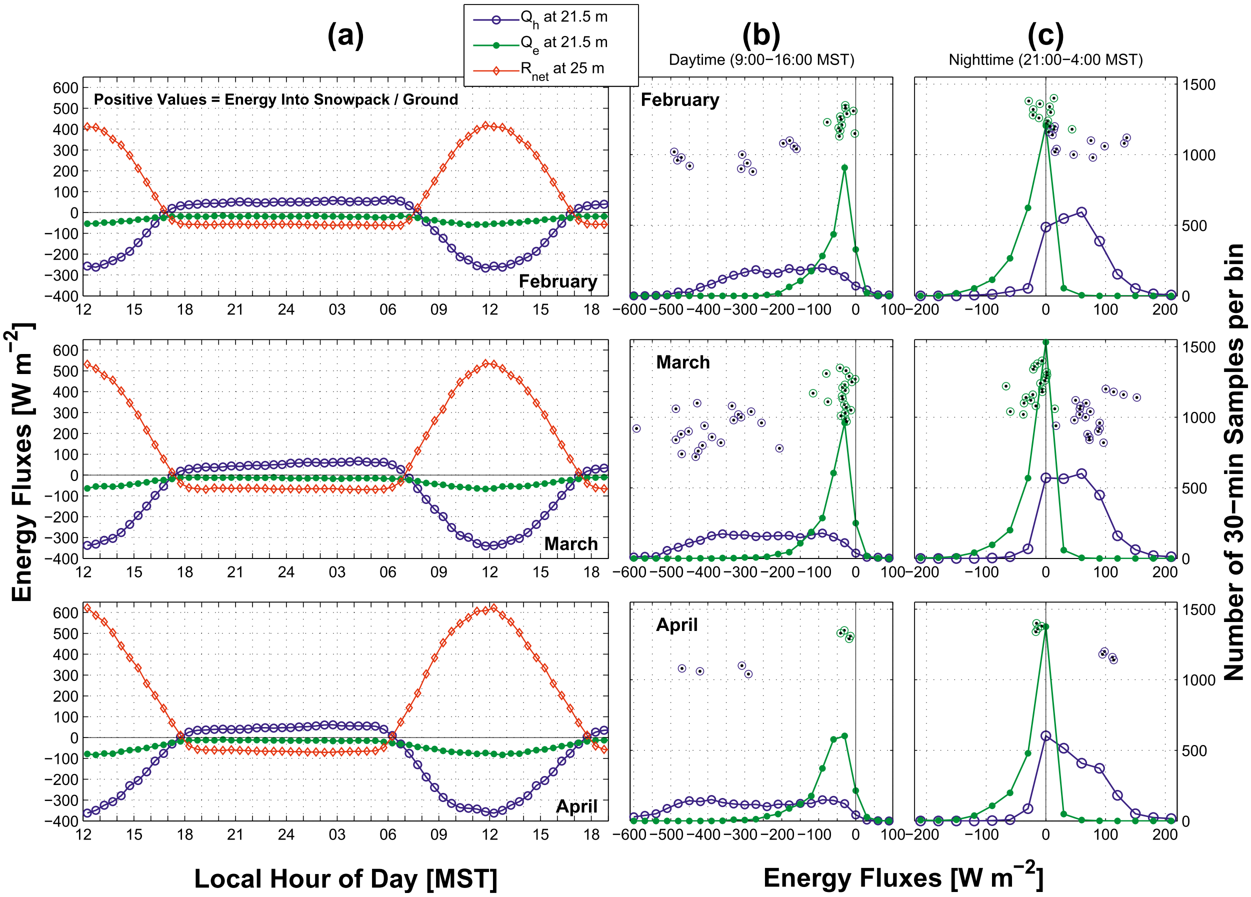

FIG. 7. Measurements of above-canopy net radiation R_{net} and sensible Q_h and latent Q_e turbulent fluxes between years 2005 and 2010 shown as monthly: (a) mean diel cycle, and frequency distributions from 30-min (b) daytime (0900–1600 MST) and (c) nighttime (2100–0400 MST) data. The legend applies to all panels. In (a), a 31-h period is shown for clarity. In (b),(c), the individual points floating above the frequency distributions are 30-min Q_h and Q_e values from the warm-up dates identified by the dashed vertical lines in Fig. 2 and listed in Table 2. In (c), the nighttime values are from the night prior to the snowpack warm-up event. Note that the x axis range in (b) is larger that of (c).

range and indicate the transfer of heat was primarily from the atmosphere to the surface (Fig. 7c).

Within the subcanopy, the latent heat flux consistently cooled the snowpack by evaporation and/or sublimation at the snow surface (qualitatively similar to above-canopy Q_e) while the soil heat flux was a steady (but small) warming of the snowpack (Fig. 8a). Subcanopy Q_h, however, is qualitatively different than above-canopy Q_h because it warmed or cooled the snow surface depending on the surrounding air (and canopy) temperature; therefore, it has a frequency distribution centered near zero (Figs. 8b,c). In general, periods with a (relatively) warm canopy were on the positive side of the Q_h frequency distributions, while those with a (relatively) cold canopy were on the negative side. Also, in the subcanopy, the shape of the Q_e and Q_h frequency distributions are similar. The change in the mean diel subcanopy Q_h flux between February and April was only on the order of 1–2 W m^{-2}.

The mean flux values during the snowpack warm-up events are listed in Table 2 and shown as individual points above the frequency distributions in Figs. 7b, 7c, 8b, and 8c. During the day of the snowpack warm-up, above-canopy Q_h and Q_e were both negative, indicating that they cooled the surface (Fig. 7b, Table 2). In the subcanopy, sensible heat was transferred to the snow surface while latent heat cooled the surface (Fig. 8b, Table 2). These results are consistent with heat being transferred away from a (relatively) warm canopy layer in both the upward and downward directions. For the fluxes on the night prior to the snowpack warm-ups, both the above-canopy (Fig. 7c) and subcanopy (Fig. 8c) sensible heat fluxes were positive (i.e., sensible heat transfer was from the atmosphere to the snowpack and forest canopy). For the pre-warm-up nights, the individual Q_e and Q_h values were typically larger (in magnitude) than the overall mean of the frequency distribution.

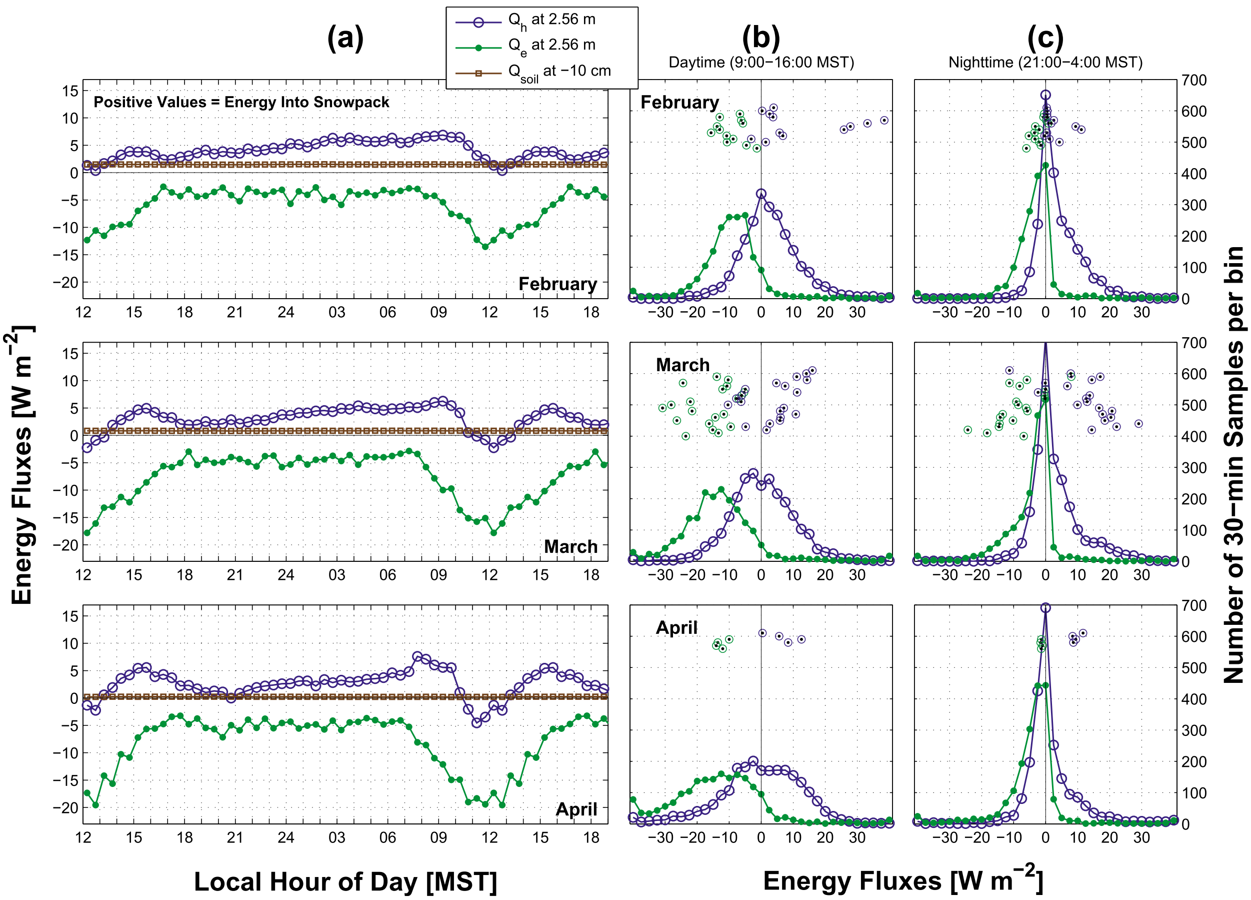

FIG. 8. As in Fig. 7, but for soil heat flux Q_{soil} and subcanopy sensible Q_h and latent Q_e turbulent fluxes.

e. Midday sensible heat flux

As shown in Fig. 8a, there was a tendency for subcanopy sensible heat flux to cool the snow surface between the hours of 1100 and 1300 mountain standard time (MST). This is surprising because midday is when the air and canopy temperature is at a near maximum, which should lead to surface warming by sensible heat. Consistent with our summary from the previous section, the midday subcanopy Q_h was strongly affected by the air/canopy temperature, with sensible heat warming the snow surface when the air temperature was the warmest (Fig. 9a). In contrast, above-canopy midday Q_h flux always transferred heat away from the surface, with stronger heat transfer occurring for warmer air temperatures. When we examine the effect of wind speed (WS) on the fluxes (Fig. 9b), both subcanopy and above-canopy Q_h were affected by low wind speeds, but beyond about 3–4 m s^{-1} there was not any dramatic change to the flux magnitude.

Near the ground, the bulk Richardson number Ri_b is often used to characterize atmospheric stability by comparing the ratio of buoyancy to wind shear (Businger 1973; Kaimal and Finnigan 1994). We calculated Ri_b between the highest (21.5 m) and lowest (2 m) measurement levels at the NWT tower with

$$\mathrm{Ri}_b = \frac{g}{\overline{T}_a}\frac{(\overline{\theta}_{21.5\,\mathrm{m}} - \overline{\theta}_{2\,\mathrm{m}})\Delta z}{(\mathrm{WS}_{21.5\,\mathrm{m}})^2}, \tag{5}$$

where g is acceleration due to gravity, $\overline{T}_a$ is the average air temperature of the layer, $\overline{\theta}$ is mean potential temperature, and Δz is the difference in height between the levels ($21.5 - 2 = 19.5$ m). Large negative Ri_b indicates unstable "free convection" conditions and small negative Ri_b indicates near-neutral conditions where strong winds create a well-mixed atmosphere. Ri_b estimates the stability between the ground and above-canopy air, not the local stability that might exist within different regions of the canopy airspace.

In windy (near neutral) conditions, the subcanopy midday heat flux tended to warm the snow surface (Fig. 9c). Strongly unstable conditions typically result in above-canopy upslope winds at the site (e.g., Burns et al. 2011), and these were the conditions when the

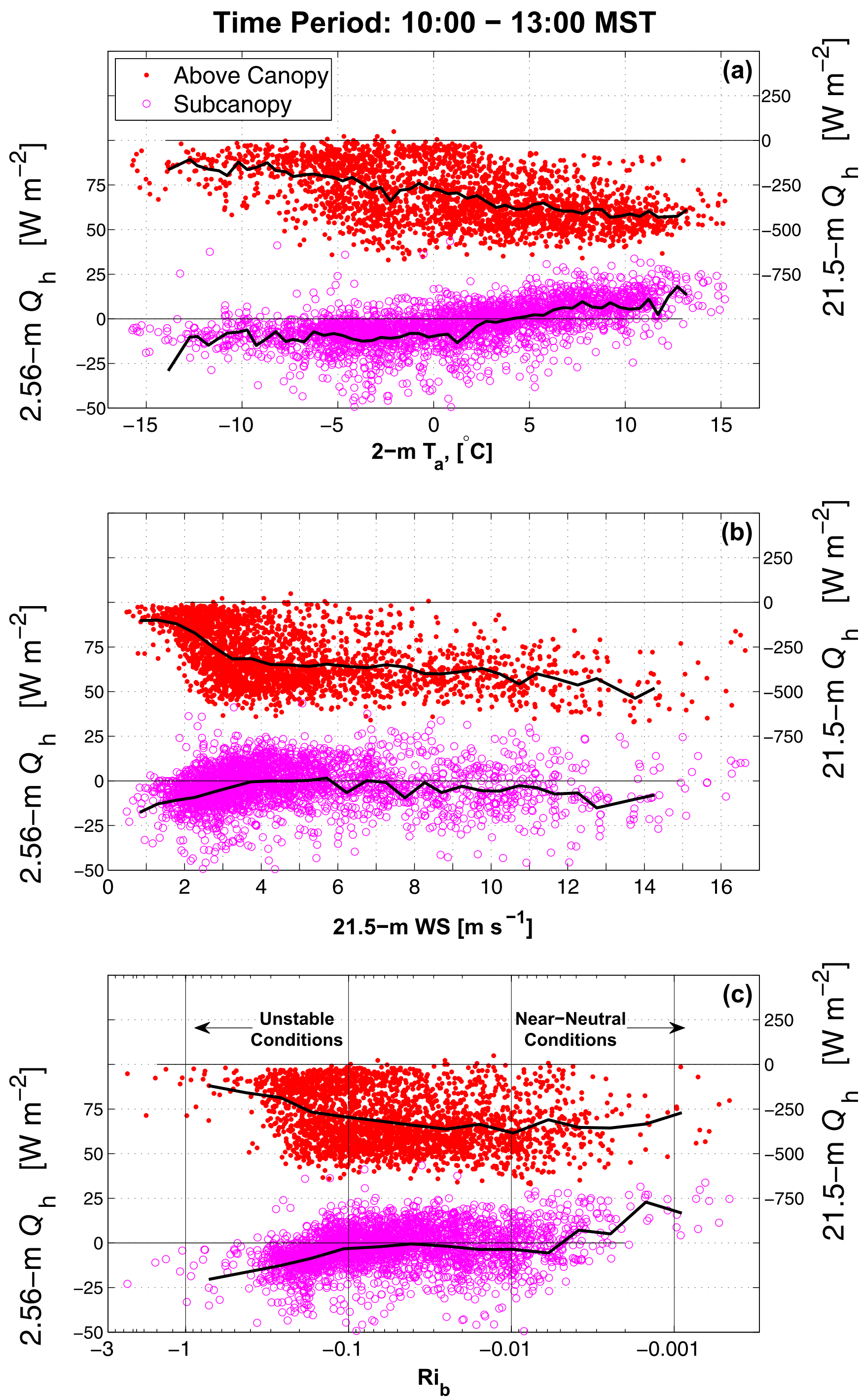

FIG. 9. The subcanopy (left axis) and above-canopy (right axis) sensible heat flux Q_h as a function of (a) 2-m air temperature T_a, (b) 21.5-m wind speed WS, and (c) bulk Richardson number Ri_b. These data are from 1000 to 1300 MST for March and April between years 2005 and 2010, and the black line is the binned mean of the 30-min values.

snow surface was cooled by subcanopy Q_h (Fig. 9c). For a deeper understanding of this situation, we examined the above-canopy and subcanopy wind directions for the three different stability regimes and found that the near-neutral regime was the only one with strong coupling between the above-canopy and subcanopy flow (Fig. 10c). Within the transitional stability regime ($-0.1 < \mathrm{Ri}_b < -0.03$), the above-canopy flow was

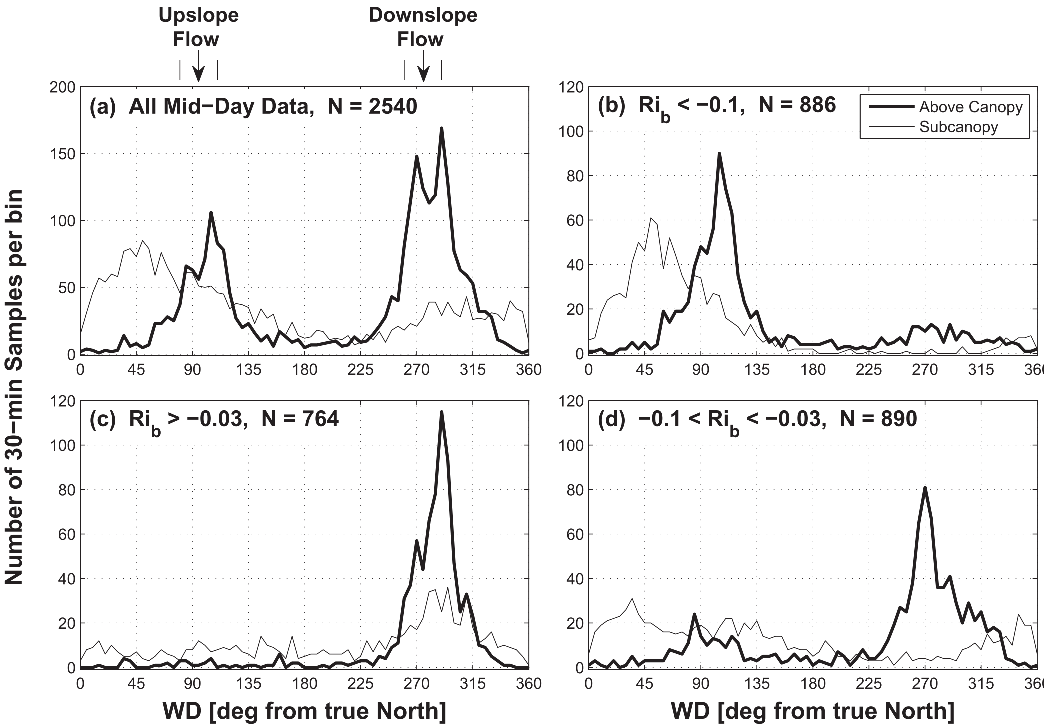

FIG. 10. Frequency distributions of midday (1000–1300 MST) above-canopy (21.5 m) and subcanopy (2.5 m) wind direction (WD) for different stability regimes based on the bulk Richardson number Ri_b, where the data selected to form the distributions are (a) all data, (b) $Ri_b < -0.1$ (unstable conditions), (c) $Ri_b > -0.03$ (near-neutral conditions), and (d) a transitional stability regime $-0.1 < Ri_b < -0.03$. These data are from March and April between years 2005 and 2010. Upslope flows are from the east and downslope flows are from the west. The legend in (b) applies to all panels, and N is the total number of 30-min samples for each distribution.

primarily downslope, whereas the subcanopy flow was upslope or from some other direction (Fig. 10d). These very different wind directions indicate some level of decoupling occurred between the above-canopy and subcanopy, similar to what was found in the summer by Burns et al. (2011). This result suggests that the negative midday subcanopy sensible heat flux shown in Fig. 8a is due to above-canopy and subcanopy decoupling. For strongly unstable conditions, we suspect other subcanopy processes may be important, which will be discussed in section 5b. Whether wind directional shear is equivalent to decoupled flow in unstable conditions remains an open question (e.g., Thomas et al. 2013).

f. An example snowpack warm-up event

In this section we focus on one 10-day period in 2006 when a sudden warm-up of the snowpack occurred and the derivative of the snowpack cold content (Q_{cc}) spiked to around 80 W m^{-2} (Fig. 11m). During this period, each day had similar clear-sky radiative conditions (Fig. 11a) and there was only one small precipitation event (Fig. 11b).

During the night prior to the snowpack warming event, there was a strong downslope wind (the so-called Chinook or Foehn wind) that prevented the near-surface air temperature from dropping below freezing and kept the subcanopy and above-canopy air well coupled (Thomas et al. 2013). The resulting ''warm'' canopy, coupled with strong winds, led to an increase in Q_h starting at around 0200 MST on 28 February (Fig. 12e). The unusual timing, duration, and magnitude of the sensible heat flux created an extended period of snowpack warming and played a part in the warming event that occurred 12 h later (as shown in Figs. 8b,c; the subcanopy Q_h values of 30 W m^{-2} are among the maximum values measured in February–April). Soil moisture sensors indicated an increase in liquid water content at the time of the T_s warm-up (Fig. 11h), so there was a large enough energy input at the snowpack surface to initiate melt and transition from a dry to wet snowpack.

On the basis of the MRC probe vertical temperature profiles (Fig. 12f), the warming of the snowpack started at the snowpack surface and propagated toward the ground. The time to warm the entire snowpack was on the order of 2 h, and after the snowpack became isothermal, there was very little variation from 0°C. On the basis of these vertical temperature profiles, the estimated travel speed of the warming front is 0.3 m h^{-1}. Though the

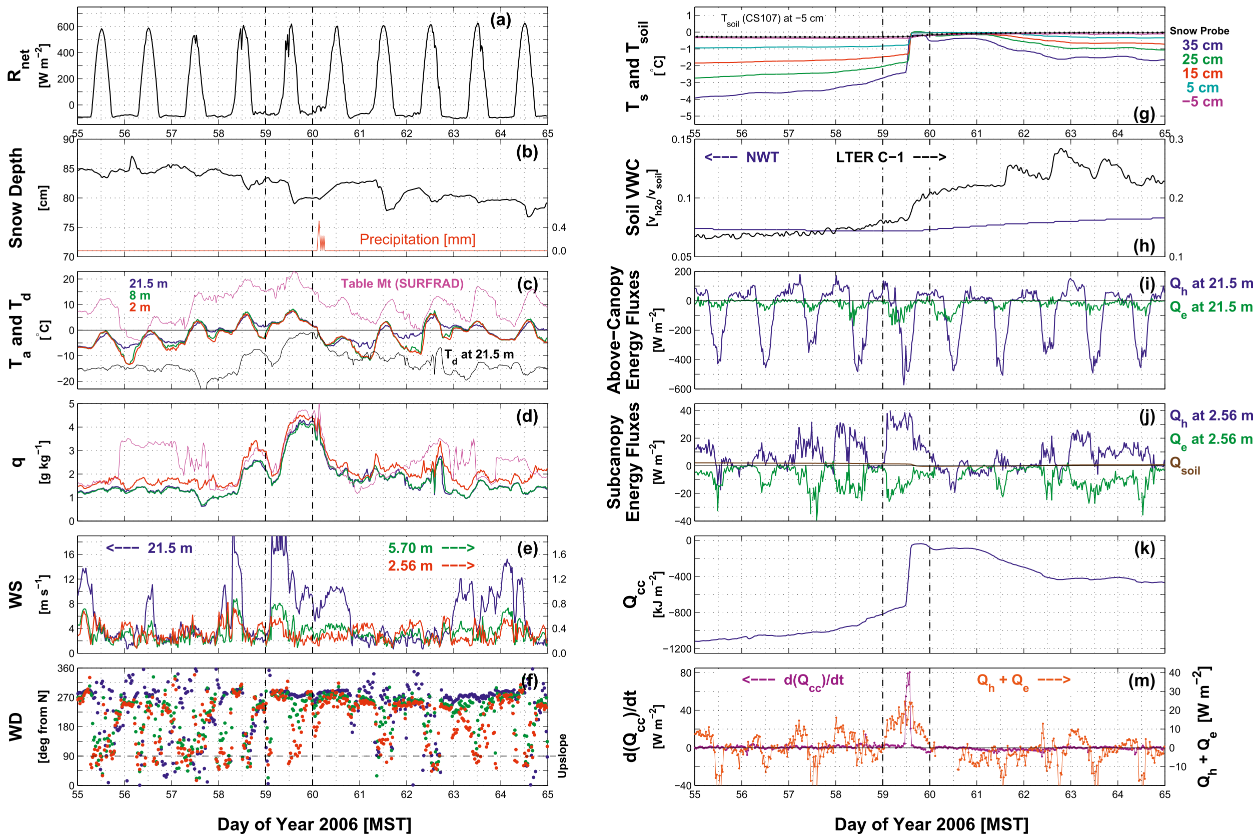

FIG. 11. The 10-day time series centered on a snowpack warm-up on 28 Feb 2006 of (a) 25-m net radiation R_{net}; (b) snow depth (at the MRC probe) and precipitation; (c) air T_a and dewpoint T_d temperature; (d) specific humidity q; (e) WS; (f) WD; (g) snow T_s and soil T_{soil} temperature; (h) soil volumetric water content (VWC); (i) above-canopy turbulent sensible Q_h and latent Q_e heat fluxes; (j) subcanopy Q_h, Q_e, and ground heat flux Q_{soil}; (k) snowpack cold-content Q_{cc}; and (m) the time derivative of cold content $d(Q_{cc})/dt$ and sum of the subcanopy turbulent fluxes. The vertical dashed lines designate the day when the snowpack warm-up occurred. In (e),(h),(m), y axis labels are on the left and right sides with arrows indicating which variables correspond to which axis. In (c),(d), T_a and q from the Table Mountain SURFRAD site at 1689-m elevation are shown. In (h), soil moisture (VWC) data from the LTER C-1 site are shown. All other data are from the NWT AmeriFlux site. The Q_{cc} in (k) is determined from Eq. (3) and uses the snow depth (h) adjusted to the MRC probe as shown in (b), the average snowpack temperature (below 55 cm) for T_s, snow density ρ_s from SNOTEL site 663 (Niwot), and the heat capacity of ice ($C_s = 2106\,\mathrm{J\,kg^{-1}\,K^{-1}}$).

warming of a snowpack is a nonhomogeneous and complex process (Colbeck 1978; Marsh and Woo 1984), our warm-front propagation speed is close to the $0.22\,\mathrm{m\,h^{-1}}$ propagation speed of meltwater within a snowpack determined by Jordan (1983). During the transition from dry to wet snow, it has been reported that sudden releases of liquid water can occur (Colbeck 1978).

5. Discussion

a. Connections between snow temperature changes, air temperature, and sensible heat flux

The transition from a cold snowpack to sustained isothermality varies from year to year (e.g., Fig. 2). Some years, such as 2007, the snowpack became isothermal and then remained isothermal throughout the melt period. More typically, there were several transitions to near isothermality followed by a return to a cold snowpack. There are several environmental conditions that lead to the snowpack warming up. The simplest situation is when the presence of warm air due to synoptic weather patterns causes the snowpack to become isothermal (Male and Granger 1981; Cline 1997). In March 2007, the mean daytime air temperature was 1.8°C and 35% of daytime periods were warmer than 5°C, which led to one single transition to an isothermal snowpack (Fig. 6b). In contrast, March 2006 had a mean daytime air temperature of −2°C and less than 8% of daytime periods were warmer than 5°C, which led to several transitions between a near-isothermal and cold snowpack (Fig. 6a).

During a warm winter day, R_{net}, subcanopy Q_h, and any possible surface condensation all act together to warm the snowpack. Above-canopy R_{net} can be fairly

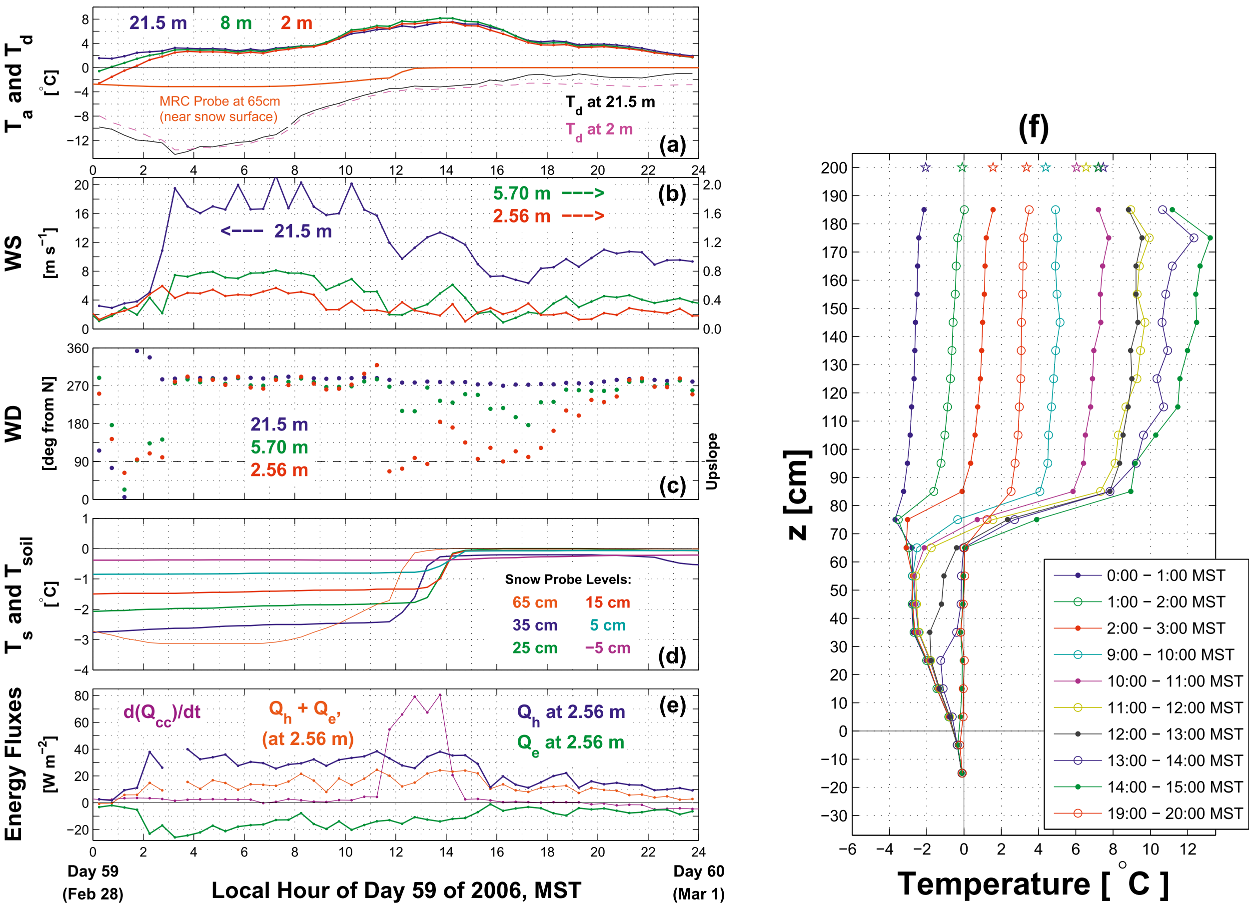

FIG. 12. The 1-day time series as the snowpack goes isothermal on 28 Feb 2006 of (a) air T_a and dewpoint T_d temperature, (b) WS, (c) WD, (d) snow and soil temperature, (e) the time derivative of snowpack cold content $d(Q_{cc})/dt$ and the 2.5 m sensible Q_h and latent Q_e heat fluxes. In (b), the 21.5-m WS is shown on the left-side axis while the other levels use the right-side axis (as indicated by the arrows). (f) Hourly vertical temperature profiles from 28 Feb 2006 for selected time periods as indicated in the legend.

similar from day to day (e.g., Fig. 11a), suggesting that it acts as a consistent forcing variable, which does not necessarily vary dramatically with synoptic air temperature, but is mostly sensitive to cloud cover. Subcanopy longwave radiation emitted by the trees, however, will be more sensitive to air temperature (Pomeroy et al. 2009). We estimated midday subcanopy net longwave radiation by using Eq. (4) and assuming that above-canopy $Q_{\mathrm{LW}}^{\downarrow}$ is 200 W m^{-2}, $F_{\mathrm{srf-c}} = 0.8$, and $\varepsilon_f = \varepsilon_{\mathrm{srf}} \approx 0.98$ (e.g., Sicart et al. 2004; DeWalle and Rango 2008). For a canopy that is 10°C warmer than the snow surface temperature (e.g., Pomeroy et al. 2009), this produces a crude estimate of $(R_{\mathrm{net}}^{\mathrm{s-c}})_{\mathrm{LW}} \approx 20$ W m^{-2}, which is similar in magnitude to our subcanopy flux measurements. This result suggests that subcanopy net longwave radiation can also be an important factor in the snowpack warm-ups.

Further evidence that large-scale air masses are responsible for the snowpack warm-ups is demonstrated by the snow temperature comparison between NWT and Soddie (Fig. 6). Though these two sites are separated by 2.5 km and have very different slope aspects, canopy structure, and wind-sheltering properties, the qualitatively similar timing of the warm-up events at Soddie and NWT is remarkable. This suggests that warm air due to synoptic weather systems is the ultimate source of snowpack warming. This does not imply that the partitioning of surface energy (or sublimation/ablation rates) at Soddie and NWT are the same. Across such a complex landscape, it is well known that the surface–atmosphere energy exchanges will vary depending on slope aspect, wind exposure, vegetation density, snow cover, and a host of other factors (e.g., Gustafson et al. 2010; Mott et al. 2011). To better understand the differences in energy partitioning at Soddie and NWT, similar instrumentation and a site-specific comparison would be necessary.

The next logical question is whether or not warmer air temperatures lead to larger eddy covariance sensible

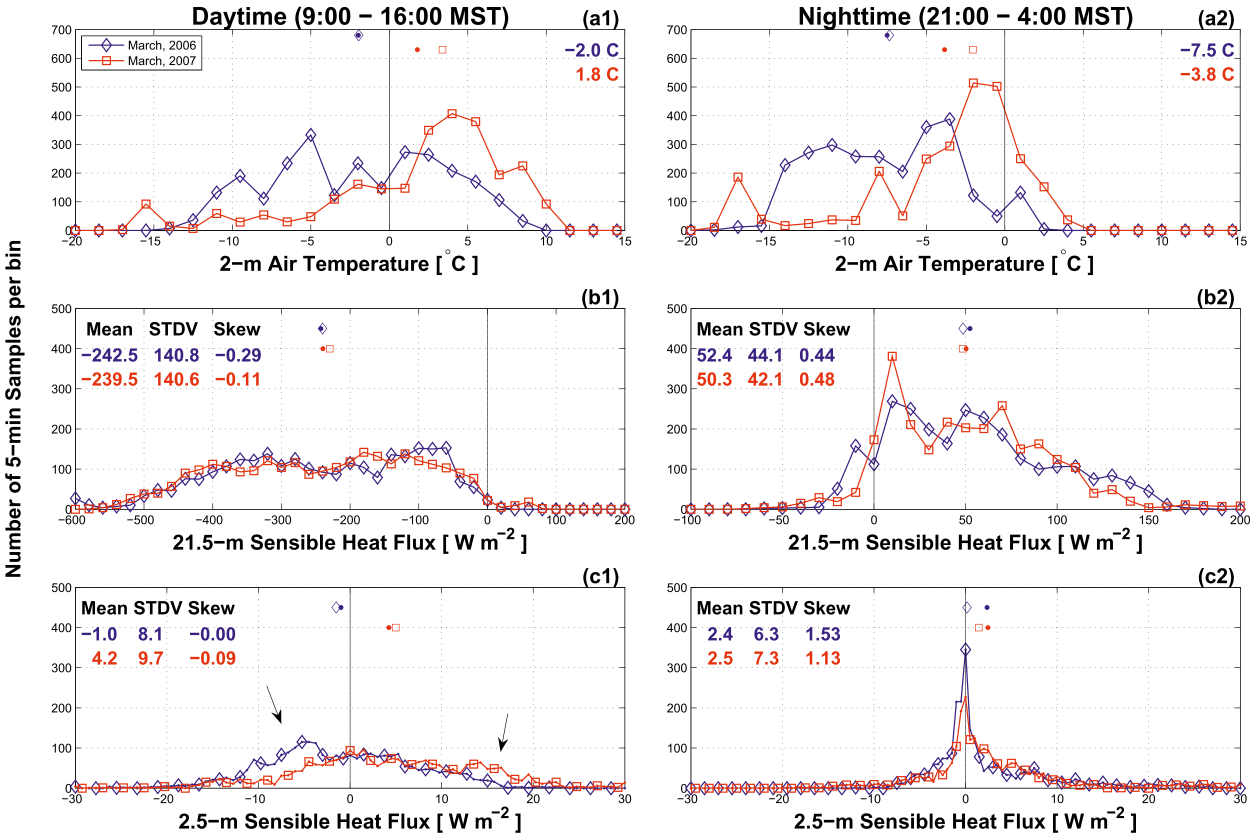

FIG. 13. Frequency distributions from March 2006 and 2007 (see legend) of: (a1),(a2) subcanopy air temperature; (b1),(b2) above-canopy sensible heat flux; and (c1),(c2) subcanopy sensible heat flux for (left) daytime (0900-1600 MST) and (right) nighttime (2100-0400 MST) periods. The mean (small filled circle) and median (open symbol) are shown floating above each frequency distribution. For the temperature panels, the means are also shown in the upper-right corner. For the heat flux panels, the means (W m^{-2}), STDVs (W m^{-2}), and skewnesses (dimensionless) are in the upper-left corner. The 5-min heat flux data are generated by linearly interpolating the 30-min heat fluxes in time. In (c1), the arrows indicate discussion points within the text.

heat fluxes. We answer this by comparing the March frequency distributions of air temperature and sensible heat flux from 2006 and 2007. Though the 2-m air temperature in 2007 (Fig. 13a1) was nearly 4°C warmer than 2006 (Fig. 13a2), the above-canopy sensible heat flux frequency distributions from 2006 and 2007 were practically indistinguishable from each other, with near-identical means, STDVs, and skewness values (Fig. 13b1,b2). This behavior can be explained if temperature changes to the tree boles, branches, and needles follow the air temperature changes such that the temperature difference between them is nearly constant. If true, this implies that the tree temperatures have a larger effect on the above-canopy Q_h magnitude than the snow surface temperature. This can be an important consideration for land surface models of snow-covered landscapes (e.g., Wang et al. 2010).

For the subcanopy fluxes, the snow cover fixes the lower surface temperature near a maximum of 0°C. Therefore, as the air–canopy temperature increases well above 0°C, the subcanopy fluxes should increase accordingly. At first glance, the subcanopy heat flux frequency distributions for 2006 (Fig. 13c1) and 2007 (Fig. 13c2) appear similar. However, the effect of the warmer air temperature in 2007 shows up in the daytime Q_h frequency distribution as a small increase in the occurrence of values between 12 and 20 W m^{-2}, whereas, for 2006, there is an increase in the Q_h occurrence between -10 and 0 W m^{-2} (as highlighted by the arrows in Fig. 13). These subtle differences result in a mean daytime subcanopy Q_h that is about 5 W m^{-2} larger in 2007 than 2006. The skewness of the daytime frequency distributions is near zero, indicating that these are near-normal frequency distributions. Because of stable nighttime conditions, the magnitudes of the 30-min nocturnal subcanopy Q_h values are smaller than daytime Q_h values, the skewness is large, and the nocturnal frequency distributions in Fig. 13c2 are more peaked around zero than those in Fig. 13c1. The mean nocturnal subcanopy Q_h values for 2006 (2.4 W m^{-2}) and 2007 (2.5 W m^{-2}) are not significantly different from each other; however, there is a still a tendency for the occurrence of more positive nocturnal Q_h values in 2007 than 2006 (Fig. 13c2).

b. Subcanopy sensible heat flux measurements

The solar radiation absorbed by the tree elements during the daytime is transferred by longwave emittance (discussed above), turbulence, or (mean) advection to the canopy airspace and snow surface. Because of the sloped topography at NWT, horizontal advection has been shown to be significant for CO_2 (Sun et al. 2007; Yi et al. 2008). For turbulence, our measurements suggest that daytime sensible heat transport is primarily from the canopy to the air immediately above the forest rather than toward the snow surface (e.g., above-canopy $Q_h \approx -200\,\mathrm{W\,m^{-2}}$ while subcanopy $Q_h \approx 4\,\mathrm{W\,m^{-2}}$). Though the warm canopy generates buoyancy and enhances turbulence above and within the canopy elements, it also creates (locally) stable conditions in the subcanopy, which suppresses turbulent mixing. The degree of subcanopy stability is largely dependent upon the magnitude and location of maximum heating within the canopy, which depends on canopy structure and sun angle (Pomeroy et al. 2009).

Subcanopy flows are affected by intermittent sweeps and ejections of above-canopy air (e.g., Finnigan 2000) that lead to weak, nonstationary flows that violate the assumptions of stationarity and homogeneity required for the eddy covariance technique (Baldocchi et al. 2000; Aubinet et al. 2012). Furthermore, subcanopy flux measurements have several additional challenges: 1) the high degree of subcanopy heterogeneity (e.g., trees and forest gaps) gives rise to dispersive fluxes (Raupach and Shaw 1982; Finnigan and Shaw 2008) that cannot be measured by a single eddy covariance flux system; 2) common flux-processing techniques, such as the planar fit (Wilczak et al. 2001; Moderow et al. 2007; Sun 2007) and using 30-min periods for flux calculations (Vickers and Mahrt 2006; Reba et al. 2009; Vickers et al. 2009), may not be applicable in the subcanopy; 3) horizontal and vertical advection of heat by the mean flow; 4) the divergence of subcanopy horizontal sensible heat flux (Staebler and Fitzjarrald 2005; Moderow et al. 2007; Serafimovich et al. 2011; Thomas 2011); 5) vertical heat flux divergence below the sonic anemometer (Mott et al. 2013); and 6) sonic anemometers that do not capture the small-scale transport because of pathlength averaging issues (Mahrt 2010). Though estimates of the momentum dispersive flux are reportedly small in the upper canopy (e.g., Poggi et al. 2004), these results depend on canopy structure (Moltchanov et al. 2011) and need to be verified for sensible heat. Though some of the issues related to small-scale and horizontal transport have been investigated over open snowfields (Parlange et al. 2007; Mott et al. 2013) and within canopies (e.g., Serafimovich et al. 2011; Patton et al. 2011; Thomas 2011), we are not aware of any study examining them within a snow-covered forest.

Our emphasis in this paper has been on the vertical heat flux (i.e., $Q_h \propto \overline{w'T'_a}$, where w' is vertical wind fluctuation and T'_a is temperature fluctuation). Within the subcanopy, the space–time relationship for wind and temperature is altered because of radiative effects on air temperature (Thomas 2011). We suspect that the divergence of the horizontal turbulent heat flux ($\overline{u'T'_a}$), where u' is streamwise wind fluctuation) and horizontal heat advection may also be significant in the subcanopy at NWT. During midday, above-canopy $\overline{u'T'_a}$ is typically 1–2 times the magnitude of $\overline{w'T'_a}$ (Wyngaard et al. 1971). Within the subcanopy, we found that midday $\overline{u'T'_a}$ was noisy with fluctuations that were a factor of 10 larger than $\overline{w'T'_a}$. We also found a seasonal dependence on the subcanopy planar-fit coefficients (results not shown) that suggests variability in the subcanopy streamlines, which are likely related to the frequency of upslope wind events and subcanopy decoupling, as discussed in section 4e. These issues (and those listed in the previous paragraph) are beyond the scope of the current study, but remain open questions regarding our subcanopy flux measurements.

c. Surface condensation effects on snow temperature changes

Though large Q_h values appear to be the primary mechanism leading to the 28 February 2006 snowpack-warming event, a closer look at Figs. 11 and 12 reveals that other factors may be playing a role. Several meteorological events occur just before the snowpack warm-up: 1) the wind speed dropped; 2) the above-canopy wind direction continued downslope, but the subcanopy wind direction switched to upslope (i.e., decoupling occurred); 3) the water vapor content of the air reached a maximum; and 4) the dewpoint temperature (T_d) approached the snow surface temperature. Upslope winds at the site can be generated by diurnal surface heating, large-scale pressure gradients, or mesoscale phenomena due to the mountainous topography (Parrish et al. 1990; Turnipseed et al. 2004), with decoupling of the above-canopy and subcanopy air occurring within the forested areas (Burns et al. 2011). In Fig. 12d, the upper snowpack temperature changes sharply just before noon, which coincides exactly with the subcanopy airflow being decoupled (Fig. 12c). There is also a corresponding change in the relative subcanopy wind speed at 2.56 m and 5.7 m (Fig. 12b) and the subcanopy sensible heat flux actually decreases (Fig. 12e). Because the sensible heat flux decreases, we suspect some

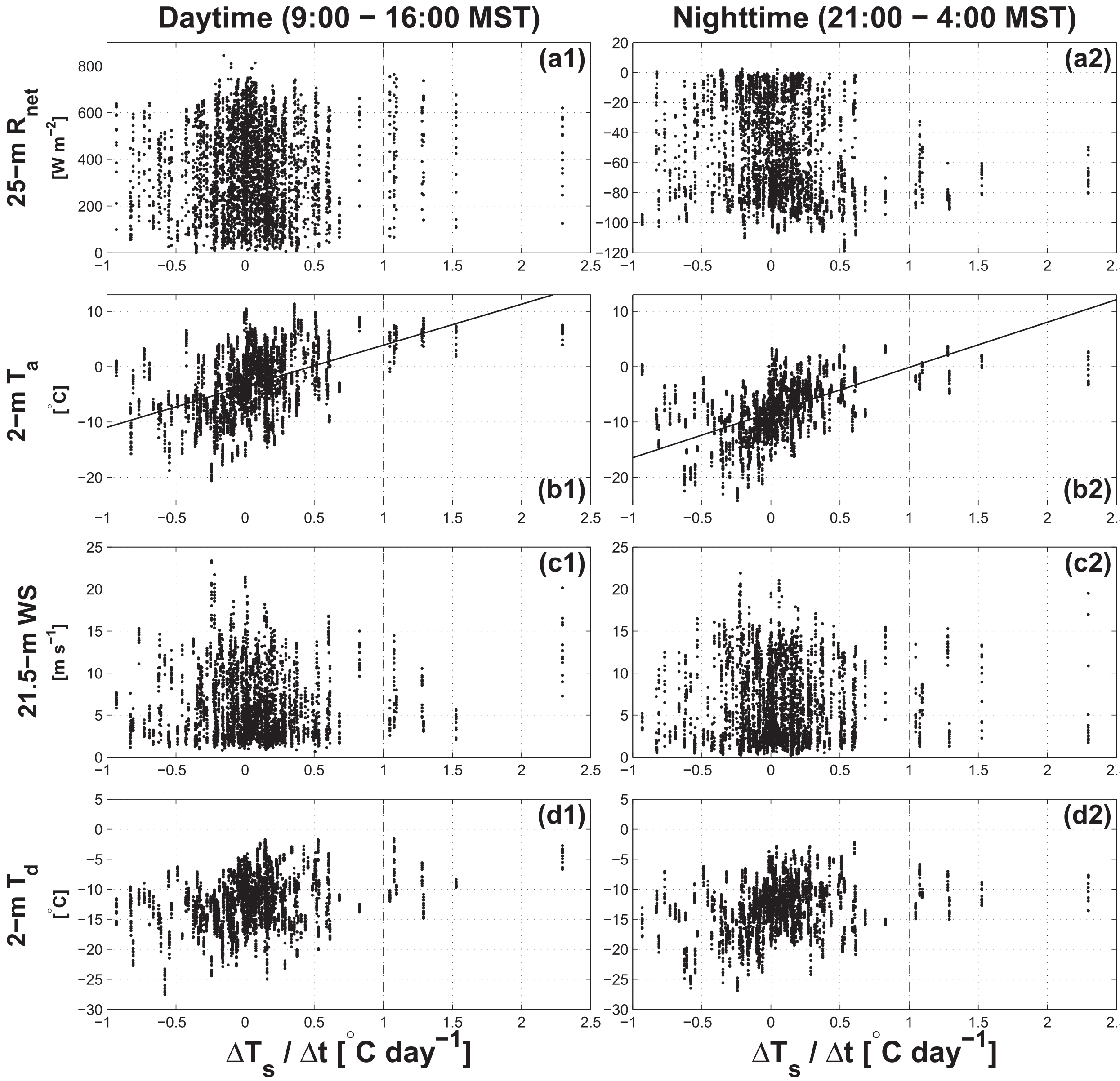

FIG. 14. The 24-h finite difference of 35-cm snow temperature ($\Delta T_s/\Delta t$, calculated from midnight to midnight) for February and March between years 2006 and 2010 vs (a1),(a2) 25-m net radiation R_{net}; (b1),(b2) subcanopy air temperature T_a; (c1),(c2) WS; and (d1),(d2) subcanopy dewpoint temperature T_d for (left) daytime (0900–1600 MST) and (right) nighttime (2100–0400 MST) periods. The vertical dashed line at $\Delta T_s/\Delta t = 1$ is the criteria used for the snowpack warm-up events. For $\Delta T_s/\Delta t < 1$, a linear fit of T_a vs $\Delta T_s/\Delta t$ is shown with slopes of 7.6 (daytime) and 8.4 (nighttime).

unmeasured phenomena (as suggested in the previous sections and within the following text) is causing the snowpack temperature to sharply increase just before noon.

Following the strong wind event during the early morning of 28 February, specific humidity q was well mixed between the NWT tower and lower-elevation SURFRAD site (Fig. 11d). Winds on the plains were upslope, indicating (relatively) warm, humid air was mixed with the air at higher elevations (Fig. 11d). These conditions can occur in winter on Niwot Ridge after a frontal system passes through the region (Parrish et al. 1990). The temperature of the snow surface at NWT was estimated to be around −2°C, which was very close to the dewpoint temperature (Fig. 12a). Dewpoint temperature is notoriously difficult to measure (e.g., Bohren and Albrecht 1998, 181–271) and is even more complicated in the subcanopy, where turbulent mixing is weak and large humidity gradients can exist between the lowest measurement-level and the air just above the snow surface (Mott et al. 2011). If air with T_d near the snow surface temperature passes over the snowpack, condensation on the snowpack surface can occur, which would release latent heat energy, warm the snowpack, and initiate snowmelt. A previous experiment near the tree line at Niwot Ridge has shown that episodic periods of net condensation can occur in midwinter (Hood et al. 1999). One could argue that condensation was not a factor in the snowpack warm-up because both subcanopy and above-canopy Q_e show evaporation occurring. However, one explanation for this apparent paradox is that Q_e was calculated from high-frequency fluctuations of q, and the advection of an air mass near the surface dewpoint temperature past the sensor would not necessarily be measured by the eddy covariance instrumentation (e.g., Finnigan 2008; Aubinet 2008).

d. *Atmospheric conditions affecting the snow temperature changes*

One of the goals of our analysis was to assess which atmospheric variables control $\Delta T_s/\Delta t$ in the snowpack. Unsurprisingly, the most important variable appears to be air temperature, with the largest warm-up events occurring for daytime air temperatures larger than 3°C (Fig. 14b1) and nighttime air temperatures that are near 0°C (Fig. 14b2). A linear fit of $\Delta T_s/\Delta t$ and T_a shows that cooling of the snowpack occurs for colder air temperatures. As shown in Fig. 14, the relationship with other environmental variables is less clear. We have shown that high winds are important for at least one of the snowpack warm-ups (i.e., as discussed in section 5c), but there does not appear to be a universal trend with wind speed (Fig. 14c1,c2), except that the cooling of the snowpack typically occurs when wind speeds are below about $10\,\mathrm{m\,s^{-1}}$. Net radiation indicates that on the night prior to the largest snowpack warm-ups, the skies are typically clear (Fig. 14a2).

Some of the snowpack warm-up events occurred gradually over a 24-h period, whereas others occurred over a shorter time period. (Table 2 lists the duration of each warm-up event.) The variability in warm-up length suggests that the physical processes controlling each individual warm-up event are unique and explains why our attempt to determine a consistent controlling factor is inconclusive. Also, our rough estimate of subcanopy net radiation shows that it can be a significant source of heat to the snowpack. Subcanopy radiation would be a useful measurement to include in any future study.

e. *Further implications*

Our study has shown that the energy balance of a high-elevation forest snowpack is often on the threshold of melting surface snow, which can lead to rapid T_s warming and the creation of a wet snowpack. Recent studies indicate a trend toward earlier snowmelt across the western United States, largely believed to be associated with increases in regional winter air temperatures (e.g., Mote et al. 2008). Here we show that atmospheric humidity may also play a role in snowpack warm-ups in continental climates where winter snowpack temperatures are well below zero.

Lazar and Williams (2008) evaluated how climate change resulting from increased greenhouse gas emissions may affect the timing of wet avalanches and snow quality at Aspen Mountain in the years 2030 and 2100. They report earlier and increased wet snow avalanches for all climate change scenarios and all years. The subalpine forest used in our study is predicted to have warmer, shorter winters in the future (Scott-Denton et al. 2013). If the rapid snowpack warm-ups shown in our study were to occur more frequently because of warmer winters, this suggests a possible mechanism for future increases in wet-snow avalanche occurrence.

6. Conclusions

Snow temperature changes within a seasonal subalpine forest snowpack were monitored for 8 yr. We found that transitions in snowpack temperature at a rate of greater than $1°\mathrm{C\,day^{-1}}$ occurred several times in late winter and early spring and were a precursor to an isothermal snowpack. Though synoptic air temperature appeared to be the primary control on the snowpack temperature, the rapid snowpack warming events were sometimes preceded by strong Chinook winds that kept the nighttime air temperature above freezing, thus creating conditions conducive to the snowpack warm-up. A simple radiation model suggests that subcanopy longwave radiative fluxes are similar in magnitude to the turbulent fluxes. However, more knowledge about the complicated radiative processes within the subcanopy is necessary.

Our results also suggest that if air with a dewpoint temperature near the snow surface temperature is present, water vapor can condense on the snow surface releasing latent heat and causing the snowpack temperature to rapidly warm. In this situation, we found that the warming front started at the snow surface and moved through the snowpack with a speed of around $0.3\,\mathrm{m\,h^{-1}}$. This type of energy transfer may not be detected by eddy covariance flux measurements because it is an advective process. We made several additional suggestions of measurement inadequacies that might exist in subcanopy flux measurements (listed in section 5b) and issues related to subcanopy decoupling. These ideas should be further tested before we can confidently use the eddy covariance technique within the subcanopy environment. Finally, we recommend that internal snowpack (and canopy) temperature measurements be included in studies of the wintertime surface energy balance, as well as studies of gas transport within a snowpack.

Acknowledgments. We gratefully acknowledge the Niwot Ridge LTER team (Jennifer Morse, Kurt Chowanski, Mark Losleben, and many others) for maintaining the LTER instruments; Jeff Beauregard for field help at the NWT site; and discussions with Dave Bowling, Don Lenschow, Ned Patton, and Jielun Sun. We also acknowledge the NRCS SNOTEL and NOAA SURFRAD networks for making their data readily available and Mage Hultstrand for providing information about the Niwot SNOTEL site. Finally, we thank three anonymous reviewers for comments that improved the manuscript. The AmeriFlux tower has been supported by two grants from the U.S. Department of Energy (DOE) [the National Institute for Climate Change Research (NICCR) and Terrestrial Carbon Processes Program (TCP)], as well as a grant from the National Science Foundation (NSF) Long-Term Research in Environmental Biology (LTREB, Grant 0918565). N.P.M. acknowledges funding from NSF EAR 1032295 and EAR 1032308. The National Center for Atmospheric Research (NCAR) is sponsored by NSF.

APPENDIX

Snowpack Thermal Diffusivity

To determine the effective thermal diffusivity $\alpha_{\rm eff}$, the heat equation [Eq. (2)] and a second-order polynomial fit to the mean T_s profile below 60 cm (shown in Fig. 6) were used. To estimate $\partial T_s/\partial t$, the mean value of $\Delta T_s/\Delta t$ between 5 and 60 cm was used (similar to what is shown in Fig. 5b, but calculated to match the time periods of Fig. 6). For years 2006, 2007, and 2009 the calculated $\alpha_{\rm eff}$ values are 3.28×10^{-7}, $2.32 \times 10^{-}$, and $1.12 \times 10^{-7}\,\mathrm{m^2\,s^{-1}}$, respectively. For a glacial seasonal snowpack in Switzerland, Oldroyd et al. (2013) calculated a median $\alpha_{\rm eff}$ of $2.5 \times 10^{-7}\,\mathrm{m^2\,s^{-1}}$ and 30-min $\alpha_{\rm eff}$ values over 2 months that ranged between 3×10^{-8} and $2 \times 10^{-6}\,\mathrm{m^2\,s^{-1}}$. This comparison shows that $\alpha_{\rm eff}$ for the NWT forest snowpack is consistent with $\alpha_{\rm eff}$ from a seasonal snowpack at a glacial site with very different characteristics.

REFERENCES

Andreas, E. L., R. E. Jordan, and A. P. Makshtas, 2004: Simulations of snow, ice, and near-surface atmospheric processes on Ice Station Weddell. *J. Hydrometeor.,* **5,** 611–624, doi:10.1175/1525-7541(2004)005<0611:SOSIAN>2.0.CO;2.

Armstrong, R. L., 1976: Wet snow avalanches. Avalanche Release and Snow Characteristics, San Juan Mountains, Colorado, Occasional Pap. 19, Institute of Arctic and Alpine Research, University of Colorado, Boulder, CO, 67–82.

Arons, E. M., and S. C. Colbeck, 1995: Geometry of heat and mass-transfer in dry snow: A review of theory and experiment. *Rev. Geophys.,* **33,** 463–493, doi:10.1029/95RG02073.

Aubinet, M., 2008: Eddy covariance CO_2 flux measurements in nocturnal conditions: An analysis of the problem. *Ecol. Appl.,* **18,** 1368–1378, doi:10.1890/06-1336.1.

——, and Coauthors, 2000: Estimates of the annual net carbon and water exchange of forests: The EUROFLUX methodology. *Adv. Ecol. Res.,* **30,** 113–175, doi:10.1016/S0065-2504(08)60018-5.

——, T. Vesala, and D. Papale, 2012: *Eddy Covariance: A Practical Guide to Measurement and Data Analysis.* Springer, 438 pp.

Baldocchi, D. D., B. E. Law, and P. M. Anthoni, 2000: On measuring and modeling energy fluxes above the floor of a homogeneous and heterogeneous conifer forest. *Agric. For. Meteor.,* **102,** 187–206, doi:10.1016/S0168-1923(00)00098-8.

Bartlett, S. J., and M. Lehning, 2011: A theoretical assessment of heat transfer by ventilation in homogeneous snowpacks. *Water Resour. Res.,* **47,** W04503, doi:10.1029/2010WR010008.

Blanken, P. D., and Coauthors, 1998: Turbulent flux measurements above and below the overstory of a boreal aspen forest. *Bound.-Layer Meteor.,* **89,** 109–140, doi:10.1023/A:1001557022310.

——, M. W. Williams, S. P. Burns, R. K. Monson, J. Knowles, K. Chowanski, and T. Ackerman, 2009: A comparison of water and carbon dioxide exchange at a windy alpine tundra and subalpine forest site near Niwot Ridge, Colorado. *Biogeochemistry,* **95,** 61–76, doi:10.1007/s10533-009-9325-9.

Bohren, C. F., and B. A. Albrecht, 1998: *Atmospheric Thermodynamics.* 1st ed. Oxford University Press, 416 pp.

Bolton, D., 1980: The computation of equivalent potential temperature. *Mon. Wea. Rev.,* **108,** 1046–1053, doi:10.1175/1520-0493(1980)108<1046:TCOEPT>2.0.CO;2.

Bowling, D. R., and W. J. Massman, 2011: Persistent wind-induced enhancement of diffusive CO_2 transport in a mountain forest snowpack. *J. Geophys. Res.,* **116,** G04006, doi:10.1029/2011JG001722.

——, ——, S. M. Schaeffer, S. P. Burns, R. K. Monson, and M. W. Williams, 2009: Biological and physical influences on the carbon isotope content of CO_2 in a subalpine forest snowpack, Niwot Ridge, Colorado. *Biogeochemistry,* **95,** 37–59, doi:10.1007/s10533-008-9233-4.

Brandt, R. E., and S. G. Warren, 1997: Temperature measurements and heat transfer in near-surface snow at the South Pole. *J. Glaciol.,* **43,** 339–351.

Burba, G. G., D. K. McDermitt, A. Grelle, D. J. Anderson, and L. K. Xu, 2008: Addressing the influence of instrument surface heat exchange on the measurements of CO_2 flux from open-path gas analyzers. *Global Change Biol.,* **14,** 1854–1876, doi:10.1111/j.1365-2486.2008.01606.x.

Burns, S. P., and Coauthors, 2011: Atmospheric stability effects on wind fields and scalar mixing within and just above a subalpine forest in sloping terrain. *Bound.-Layer Meteor.,* **138,** 231–262, doi:10.1007/s10546-010-9560-6.

——, T. W. Horst, L. Jacobsen, P. D. Blanken, and R. K. Monson, 2012: Using sonic anemometer temperature to measure sensible heat flux in strong winds. *Atmos. Meas. Tech.,* **5,** 2095–2111, doi:10.5194/amt-5-2095-2012.

Businger, J. A., 1973: Turbulent transfer in the atmospheric surface layer. *Workshop on Micrometeorology,* D. A. Haugen, Ed., Amer. Meteor. Soc., 67–100.

Clarke, G. K. C., and E. D. Waddington, 1991: A three-dimensional theory of wind pumping. *J. Glaciol.,* **37,** 89–96.

Cline, D. W., 1997: Snow surface energy exchanges and snowmelt at a continental, midlatitude alpine site. *Water Resour. Res.,* **33,** 689–701, doi:10.1029/97WR00026.

Clow, D. W., 2010: Changes in the timing of snowmelt and streamflow in Colorado: A response to recent warming. *J. Climate,* **23,** 2293–2306, doi:10.1175/2009JCLI2951.1.

Colbeck, S. C., 1978: The physical aspects of water flow through snow. *Advances in Hydroscience,* Vol. 11, V. T. Chow, Ed., Academic Press, 165–206.

——, 1989: Air movement in snow due to windpumping. *J. Glaciol.,* **35,** 209–213.

——, 1991: The layered character of snow covers. *Rev. Geophys.,* **29,** 81–96, doi:10.1029/90RG02351.

DeWalle, D., and A. Rango, 2008: *Principles of Snow Hydrology.* Cambridge University Press, 428 pp.

Domine, F., M. Albert, T. Huthwelker, H. W. Jacobi, A. A. Kokhanovsky, M. Lehning, G. Picard, and W. R. Simpson, 2008: Snow physics as relevant to snow photochemistry. *Atmos. Chem. Phys.,* **8,** 171–208, doi:10.5194/acp-8-171-2008.

Fierz, C., 2011: Temperature profile of snowpack. *Encyclopedia of Snow, Ice and Glaciers,* V. Singh, P. Singh, and U. Haritashya, Eds., Encyclopedia of Earth Sciences Series, Springer, 1151–1154.

Finnigan, J., 2000: Turbulence in plant canopies. *Annu. Rev. Fluid Mech.,* **32,** 519–571, doi:10.1146/annurev.fluid.32.1.519.

——, 2008: An introduction to flux measurements in difficult conditions. *Ecol. Appl.,* **18,** 1340–1350, doi:10.1890/07-2105.1.

——, and R. H. Shaw, 2008: Double-averaging methodology and its application to turbulent flow in and above vegetation canopies. *Acta Geophys.,* **56,** 534–561, doi:10.2478/s11600-008-0034-x.

Foken, T., M. Aubinet, and R. Leuning, 2012: The eddy covariance method. *Eddy Covariance: A Practical Guide to Measurement and Data Analysis,* M. Aubinet, T. Vesala, and D. Papale, Eds., Springer, 1–20.

Ge, Y., and G. Gong, 2010: Land surface insulation response to snow depth variability. *J. Geophys. Res.,* **115,** D08107, doi:10.1029/2009JD012798.

Gustafson, J. R., P. D. Brooks, N. P. Molotch, and W. C. Veatch, 2010: Estimating snow sublimation using natural chemical and isotopic tracers across a gradient of solar radiation. *Water Resour. Res.,* **46,** W12511, doi:10.1029/2009WR009060.

Hawkins, T. W., and A. Walton, 2007: A case study of the energy budget of a snowpack in the arid, subtropical climate of the southwestern United States. *J. Ariz. Nev. Acad. Sci.,* **39,** 1–13, doi:10.2181/1533-6085(2007)39[1:ACSOTE]2.0.CO;2.

Hayashi, M., T. Hirota, Y. Iwata, and I. Takayabu, 2005: Snowmelt energy balance and its relation to Foehn events in Tokachi, Japan. *J. Meteor. Soc. Japan,* **83,** 783–798, doi:10.2151/jmsj.83.783.

Heywood, L., 1989: Wet snow avalanches stability evaluation and control. *Avalanche Rev.,* **7,** 1–7.

Hicks, B., and H. Martin, 1972: Atmospheric turbulent fluxes over snow. *Bound.-Layer Meteor.,* **2,** 496–502, doi:10.1007/BF00821551.

Hood, E., M. Williams, and D. Cline, 1999: Sublimation from a seasonal snowpack at a continental, mid-latitude alpine site. *Hydrol. Processes,* **13,** 1781–1797, doi:10.1002/(SICI)1099-1085(199909)13:12/13<1781::AID-HYP860>3.0.CO;2-C.

Hu, J., D. J. P. Moore, S. P. Burns, and R. K. Monson, 2010: Longer growing seasons lead to less carbon sequestration by a subalpine forest. *Global Change Biol.,* **16,** 771–783, doi:10.1111/j.1365-2486.2009.01967.x.

Jordan, P., 1983: Meltwater movement in a deep snowpack: 1. Field observations. *Water Resour. Res.,* **19,** 971–978, doi:10.1029/WR019i004p00971.

Kaempfer, T. U., M. Schneebeli, and S. A. Sokratov, 2005: A microstructural approach to model heat transfer in snow. *Geophys. Res. Lett.,* **32,** L21503, doi:10.1029/2005GL023873.

Kaimal, J. C., and J. J. Finnigan, 1994: *Atmospheric Boundary Layer Flows: Their Structure and Measurement.* Oxford University Press, 289 pp.

Knowles, J. F., P. D. Blanken, M. W. Williams, and K. M. Chowanski, 2012: Energy and surface moisture seasonally limit evaporation and sublimation from snow-free alpine tundra. *Agric. For. Meteor.,* **157,** 106–115, doi:10.1016/j.agrformet.2012.01.017.

Langham, E. J., 1981: Physics and properties of snowcover. *Handbook of Snow: Principles, Processes, Management & Use,* D. M. Gray and D. H. Male, Eds., Pergamon Press, 275–337.

Lawler, R. R., and T. E. Link, 2011: Quantification of incoming all-wave radiation in discontinuous forest canopies with application to snowmelt prediction. *Hydrol. Processes,* **25,** 3322–3331, doi:10.1002/hyp.8150.

Lazar, B., and M. Williams, 2008: Climate change in western ski areas: Potential changes in the timing of wet avalanches and snow quality for the aspen ski area in the years 2030 and 2100. *Cold Reg. Sci. Technol.,* **51,** 219–228, doi:10.1016/j.coldregions.2007.03.015.

Mahrt, L., 2010: Computing turbulent fluxes near the surface: Needed improvements. *Agric. For. Meteor.,* **150,** 501–509, doi:10.1016/j.agrformet.2010.01.015.

——, and D. Vickers, 2005: Moisture fluxes over snow with and without protruding vegetation. *Quart. J. Roy. Meteor. Soc.,* **131,** 1251–1270, doi:10.1256/qj.04.66.

Male, D. H., and R. J. Granger, 1981: Snow surface-energy exchange. *Water Resour. Res.,* **17,** 609–627, doi:10.1029/WR017i003p00609.

Marks, D., and J. Dozier, 1992: Climate and energy exchange at the snow surface in the alpine region of the Sierra Nevada: 2. Snow cover energy-balance. *Water Resour. Res.,* **28,** 3043–3054, doi:10.1029/92WR01483.

——, M. Reba, J. Pomeroy, T. Link, A. Winstral, G. Flerchinger, and K. Elder, 2008: Comparing simulated and measured sensible and latent heat fluxes over snow under a pine canopy to improve an energy balance snowmelt model. *J. Hydrometeor.,* **9,** 1506–1522, doi:10.1175/2008JHM874.1.

Marsh, P., and M. K. Woo, 1984: Wetting front advance and freezing of meltwater within a snow cover. 1. Observations in the Canadian arctic. *Water Resour. Res.,* **20,** 1853–1864, doi:10.1029/WR020i012p01853.

——, and J. W. Pomeroy, 1996: Meltwater fluxes at an arctic forest-tundra site. *Hydrol. Processes,* **10,** 1383–1400, doi:10.1002/(SICI)1099-1085(199610)10:10<1383::AID-HYP468>3.0.CO;2-W.

Marty, C., 2008: Regime shift of snow days in Switzerland. *Geophys. Res. Lett.,* **35,** L12501, doi:10.1029/2008GL033998.

Massman, W. J., and X. Lee, 2002: Eddy covariance flux corrections and uncertainties in long term studies of carbon and energy exchanges. *Agric. For. Meteor.,* **113,** 121–144, doi:10.1016/S0168-1923(02)00105-3.

——, R. A. Sommerfeld, A. R. Mosier, K. F. Zeller, T. J. Hehn, and S. G. Rochelle, 1997: A model investigation of turbulence-driven pressure-pumping effects on the rate of diffusion of CO_2, N_2O, and CH_4 through layered snowpacks. *J. Geophys. Res.,* **102,** 18 851–18 863, doi:10.1029/97JD00844.

McClung, D., 1996: Effects of temperature on fracture in dry slab avalanche release. *J. Geophys. Res.,* **101,** 21 907–21 920, doi:10.1029/95JB03114.

——, and P. Schaerer, 2006: *The Avalanche Handbook.* 3rd ed. The Mountaineers, 324 pp.

McKay, D. C., and G. W. Thurtell, 1978: Measurements of energy fluxes involved in energy budget of a snow cover. *J. Appl. Meteor.,* **17,** 339–349, doi:10.1175/1520-0450(1978)017<0339:MOTEFI>2.0.CO;2.

Moderow, U., C. Feigenwinter, and C. Bernhofer, 2007: Estimating the components of the sensible heat budget of a tall forest canopy in complex terrain. *Bound.-Layer Meteor.,* **123,** 99–120, doi:10.1007/s10546-006-9136-7.

Molotch, N. P., P. D. Blanken, M. W. Williams, A. A. Turnipseed, R. K. Monson, and S. A. Margulis, 2007: Estimating sublimation of intercepted and sub-canopy snow using eddy covariance systems. *Hydrol. Processes,* **21,** 1567–1575, doi:10.1002/hyp.6719.

——, P. D. Brooks, S. P. Burns, M. Litvak, R. K. Monson, J. R. McConnell, and K. Musselman, 2009: Ecohydrological controls on snowmelt partitioning in mixed-conifer sub-alpine forests. *Ecohydrology,* **2,** 129–142, doi:10.1002/eco.48.

Moltchanov, S., Y. Bohbot-Raviv, and U. Shavit, 2011: Dispersive stresses at the canopy upstream edge. *Bound.-Layer Meteor.,* **139,** 333–351, doi:10.1007/s10546-010-9582-0.

Monson, R. K., and Coauthors, 2005: Climatic influences on net ecosystem CO_2 exchange during the transition from wintertime carbon source to springtime carbon sink in a high-elevation, subalpine forest. *Oecologia,* **146,** 130–147, doi:10.1007/s00442-005-0169-2.

——, A. A. Turnipseed, J. P. Sparks, P. C. Harley, L. E. Scott-Denton, K. Sparks, and T. E. Huxman, 2002: Carbon sequestration in a high-elevation, subalpine forest. *Global Change Biol.,* **8,** 459–478, doi:10.1046/j.1365-2486.2002.00480.x.

Montesi, J., K. Elder, R. A. Schmidt, and R. E. Davis, 2004: Sublimation of intercepted snow within a subalpine forest canopy at two elevations. *J. Hydrometeor.,* **5,** 763–773, doi:10.1175/1525-7541(2004)005<0763:SOISWA>2.0.CO;2.

Mote, P., A. Hamlet, and E. Salathe, 2008: Has spring snowpack declined in the Washington Cascades? *Hydrol. Earth Syst. Sci.,* **12,** 193–206, doi:10.5194/hess-12-193-2008.

Mott, R., L. Egli, T. Grunewald, N. Dawes, C. Manes, M. Bavay, and M. Lehning, 2011: Micrometeorological processes driving snow ablation in an alpine catchment. *Cryosphere,* **5,** 1083–1098, doi:10.5194/tc-5-1083-2011.

——, C. Gromke, T. Grunewald, and M. Lehning, 2013: Relative importance of advective heat transport and boundary layer decoupling in the melt dynamics of a patchy snow cover. *Adv. Water Resour.,* **55,** 88–97, doi:10.1016/j.advwatres.2012.03.001.

Musselman, K. N., N. P. Molotch, S. A. Margulis, P. B. Kirchner, and R. C. Bales, 2012a: Influence of canopy structure and direct beam solar irradiance on snowmelt rates in a mixed conifer forest. *Agric. For. Meteor.,* **161,** 46–56, doi:10.1016/j.agrformet.2012.03.011.

——, ——, ——, M. Lehning, and D. Gustafsson, 2012b: Improved snowmelt simulations with a canopy model forced with photo-derived direct beam canopy transmissivity. *Water Resour. Res.,* **48,** W10509, doi:10.1029/2012WR012285.

Niederdorfer, E., 1933: Messungen des wärmeumsatzes über schneebedecktem boden (Measurements of heat exchange over a snow-covered ground). *Meteor. Z.,* **50,** 201–208.

NOAA, cited 2012: Data from the SURFRAD Network. [Available online at http://www.esrl.noaa.gov/gmd/grad/surfrad/.]

Oldroyd, H. J., C. W. Higgins, H. Huwald, J. S. Selker, and M. B. Parlange, 2013: Thermal diffusivity of seasonal snow determined from temperature profiles. *Adv. Water Resour.,* **55,** 121–130, doi:10.1016/j.advwatres.2012.06.011.

Parlange, M. B., E. Bou-Zeid, H. Huwald, M. Chamecki, and C. Meneveau, 2007: SNOHATS: Stratified atmospheric turbulence over snow surfaces. *Advances in Turbulence XI,* J. Palma and A. Lopes, Eds., Springer Berlin Heidelberg, 520–522.

Parrish, D. D., and Coauthors, 1990: Systematic variations in the concentration of NO_x (NO plus NO_2) at Niwot Ridge, Colorado. *J. Geophys. Res.,* **95,** 1817–1836, doi:10.1029/JD095iD02p01817.

Patton, E. G., and Coauthors, 2011: The Canopy Horizontal Array Turbulence Study. *Bull. Amer. Meteor. Soc.,* **92,** 593–611, doi:10.1175/2010BAMS2614.1.

Pepin, N. C., and J. D. Lundquist, 2008: Temperature trends at high elevations: Patterns across the globe. *Geophys. Res. Lett.,* **35,** L14701, doi:10.1029/2008GL034026.

Pfeffer, W. T., and N. F. Humphrey, 1996: Determination of timing and location of water movement and ice-layer formation by temperature measurements in sub-freezing snow. *J. Glaciol.,* **42,** 292–304.

Poggi, D., G. G. Katul, and J. D. Albertson, 2004: Momentum transfer and turbulent kinetic energy budgets within a dense model canopy. *Bound.-Layer Meteor.,* **111,** 589–614, doi:10.1023/B:BOUN.0000016502.52590.af.

Pomeroy, J. W., and E. Brun, 1999: Physical properties of snow. *Snow Ecology,* H. G. Jones et al., Eds., Cambridge University Press, 45–126.

——, D. Marks, T. Link, C. Ellis, J. Hardy, A. Rowlands, and R. Granger, 2009: The impact of coniferous forest temperature on incoming longwave radiation to melting snow. *Hydrol. Processes,* **23,** 2513–2525, doi:10.1002/hyp.7325.

Raupach, M. R., and R. H. Shaw, 1982: Averaging procedures for flow within vegetation canopies. *Bound.-Layer Meteor.,* **22,** 79–90, doi:10.1007/BF00128057.

Reba, M. L., T. E. Link, D. Marks, and J. Pomeroy, 2009: An assessment of corrections for eddy covariance measured turbulent fluxes over snow in mountain environments. *Water Resour. Res.,* **45,** W00D38, doi:10.1029/2008WR007045.

Reusser, D. E., and E. Zehe, 2011: Low-cost monitoring of snow height and thermal properties with inexpensive temperature sensors. *Hydrol. Processes,* **25,** 1841–1852, doi:10.1002/hyp.7937.

Reverter, B. R., E. P. Sánchez-Cañete, V. Resco, P. Serrano-Ortiz, C. Oyonarte, and A. S. Kowalski, 2010: Analyzing the major drivers of NEE in a Mediterranean alpine shrubland. *Biogeosciences,* **7,** 2601–2611, doi:10.5194/bg-7-2601-2010.

Schlatter, T. W., 1972: The local surface energy balance and subsurface temperature regime in antarctica. *J. Appl. Meteor.,* **11,** 1048–1062, doi:10.1175/1520-0450(1972)011<1048:TLSEBA>2.0.CO;2.

Schweizer, J., J. B. Jamieson, and M. Schneebeli, 2003: Snow avalanche formation. *Rev. Geophys.,* **41,** 1016, doi:10.1029/2002RG000123.

Scott-Denton, L. E., D. J. P. Moore, N. A. Rosenbloom, T. G. F. Kittel, S. P. Burns, D. S. Schimel, and R. K. Monson, 2013:

Forecasting net ecosystem CO_2 exchange in a subalpine forest using model data assimilation combined with simulated climate and weather generation. *J. Geophys. Res. Biogeosci.,* **118,** 549–565, doi:10.1002/jgrg.20039.

Seok, B., D. Helmig, M. W. Williams, D. Liptzin, K. Chowanski, and J. Hueber, 2009: An automated system for continuous measurements of trace gas fluxes through snow: An evaluation of the gas diffusion method at a subalpine forest site, Niwot Ridge, Colorado. *Biogeochemistry,* **95,** 95–113, doi:10.1007/s10533-009-9302-3.

Serafimovich, A., C. Thomas, and T. Foken, 2011: Vertical and horizontal transport of energy and matter by coherent motions in a tall spruce canopy. *Bound.-Layer Meteor.,* **140,** 429–451, doi:10.1007/s10546-011-9619-z.

Sicart, J. E., J. W. Pomeroy, R. L. H. Essery, J. Hardy, T. Link, and D. Marks, 2004: A sensitivity study of daytime net radiation during snowmelt to forest canopy and atmospheric conditions. *J. Hydrometeor.,* **5,** 774–784, doi:10.1175/1525-7541(2004)005<0774:ASSODN>2.0.CO;2.

Staebler, R. M., and D. R. Fitzjarrald, 2005: Measuring canopy structure and the kinematics of subcanopy flows in two forests. *J. Appl. Meteor.,* **44,** 1161–1179, doi:10.1175/JAM2265.1.

Strack, J. E., G. E. Liston, and R. A. Pielke, 2004: Modeling snow depth for improved simulation of snow-vegetation-atmosphere interactions. *J. Hydrometeor.,* **5,** 723–734, doi:10.1175/1525-7541(2004)005<0723:MSDFIS>2.0.CO;2.

Sturm, M., and J. B. Johnson, 1991: Natural convection in the subarctic snow cover. *J. Geophys. Res.,* **96,** 11 657–11 671, doi:10.1029/91JB00895.

——, J. Holmgren, M. Konig, and K. Morris, 1997: The thermal conductivity of seasonal snow. *J. Glaciol.,* **43,** 26–41.

——, D. K. Perovich, and J. Holmgren, 2002: Thermal conductivity and heat transfer through the snow on the ice of the Beaufort Sea. *J. Geophys. Res.,* **107,** 8043, doi:10.1029/2000JC000409.

Sun, J., 2007: Tilt corrections over complex terrain and their implication for CO_2 transport. *Bound.-Layer Meteor.,* **124,** 143–159, doi:10.1007/s10546-007-9186-5.

——, and Coauthors, 2007: CO_2 transport over complex terrain. *Agric. For. Meteor.,* **145,** 1–21, doi:10.1016/j.agrformet.2007.02.007.

Sverdrup, H. U., 1936: The eddy conductivity of the air over a smooth snow field: Results of the Norwegian-Swedish Spitsbergen Expedition in 1934. *Geofys. Publ.,* **XI** (7), 69 pp.

Takahashi, Y., S. Soma, S. Nemoto, Y. Miyata, H. Tokitue, and T. Kudo, 1956: Observations and a theory of temperature profiles in a surface layer of snow cooling through nocturnal radiation. *J. Japanese Soc. Snow Ice,* **18,** 43–47, doi:10.5331/seppyo.18.43.

Thomas, C. K., 2011: Variability of sub-canopy flow, temperature, and horizontal advection in moderately complex terrain. *Bound.-Layer Meteor.,* **139,** 61–81, doi:10.1007/s10546-010-9578-9.

——, J. G. Martin, B. E. Law, and K. Davis, 2013: Toward biologically meaningful net carbon exchange estimates for tall, dense canopies: Multi-level eddy covariance observations and canopy coupling regimes in a mature Douglas-fir forest in Oregon. *Agric. For. Meteor.,* **173,** 14–27, doi:10.1016/j.agrformet.2013.01.001.

Turnipseed, A. A., P. D. Blanken, D. E. Anderson, and R. K. Monson, 2002: Energy budget above a high-elevation subalpine forest in complex topography. *Agric. For. Meteor.,* **110,** 177–201, doi:10.1016/S0168-1923(01)00290-8.

——, D. E. Anderson, S. Burns, P. D. Blanken, and R. K. Monson, 2004: Airflows and turbulent flux measurements in mountainous terrain. Part 2: Mesoscale effects. *Agric. For. Meteor.,* **125,** 187–205, doi:10.1016/j.agrformet.2004.04.007.

Vickers, D., and L. Mahrt, 2006: A solution for flux contamination by mesoscale motions with very weak turbulence. *Bound.-Layer Meteor.,* **118,** 431–447, doi:10.1007/s10546-005-9003-y.

——, C. Thomas, and B. E. Law, 2009: Random and systematic CO_2 flux sampling errors for tower measurements over forests in the convective boundary layer. *Agric. For. Meteor.,* **149,** 73–83, doi:10.1016/j.agrformet.2008.07.005.

Wang, Z., X. Zeng, and M. Decker, 2010: Improving snow processes in the Noah land model. *J. Geophys. Res.,* **115,** D20108, doi:10.1029/2009JD013761.

Wilczak, J. M., S. P. Oncley, and S. A. Stage, 2001: Sonic anemometer tilt correction algorithms. *Bound.-Layer Meteor.,* **99,** 127–150, doi:10.1023/A:1018966204465.

Williams, M. W., D. Helmig, and P. Blanken, 2009: White on green: Under-snow microbial processes and trace gas fluxes through snow, Niwot Ridge, Colorado Front Range. *Biogeochemistry,* **95,** 1–12, doi:10.1007/s10533-009-9330-z.

Wyngaard, J. C., O. R. Cote, and Y. Izumi, 1971: Local free convection, similarity, and budgets of shear stress and heat flux. *J. Atmos. Sci.,* **28,** 1171–1182, doi:10.1175/1520-0469(1971)028<1171:LFCSAT>2.0.CO;2.

Yen, Y.-C., 1995: Sensible heat flux measurements near a cold surface. CRREL Rep. 95-22, Cold Regions Research & Engineering Laboratory, U.S. Army Corps of Engineers, Hanover, NH, 43 pp. [Available online at http://www.dtic.mil/dtic/tr/fulltext/u2/a353423.pdf.]

Yi, C., D. E. Anderson, A. A. Turnipseed, S. P. Burns, J. P. Sparks, D. I. Stannard, and R. K. Monson, 2008: The contribution of advective fluxes to net ecosystem exchange in a high-elevation, subalpine forest. *Ecol. Appl.,* **18,** 1379–1390, doi:10.1890/06-0908.1.